PERFORMANCE OF JAROSITE BASED CONCRETE

A DISSERTATION

Submitted in partial fulfilment of the

requirements for the award of the degree

of

MASTER OF TECHNOLOGY

in

CIVIL ENGINEERING

(With Specialization in Structural Engineering)

By

LUBWAMA DAUDI

(17523012)

DEPARTMENT OF CIVIL ENGINEERING

INDIAN INSTITUTE OF TECHNOLOGY ROORKEE

ROORKEE – 247667 (INDIA)

JUNE, 2019

DECLARATION

I hereby declare that the work presented in this dissertation entitled **"PERFORMANCE OF JAROSITE BASED CONCRETE**" submitted to the Department of Civil Engineering at Indian Institute of Technology Roorkee is an authentic record of my own work carried out under the guidance of **Dr. Sonalisa Ray**, Assistant Professor, Department of Civil Engineering, Indian Institute of Technology Roorkee, India.

The content of this dissertation has never been submitted to any institution for the award of a certificate, diploma or degree and therefore an original copy.

Date: Lubwama Daudi

Place: Roorkee 17523012

CERTIFICATION

This is to certify that the above statement made by this candidate is correct to the best of my knowledge and belief.

Date:

Dr. Sonalisa Ray

Assistant Professor,

Department of Civil Engineering,

Indian Institute of Technology Roorkee

ACKNOWLEDGEMENT

I wish to express my deep sense of gratitude and sincere thanks to my supervisor Dr. Sonalisa Ray, Assistant professor, Department of Civil Engineering, IIT Roorkee for her consistent supervision and guidance towards the successful completion of this dissertation project. Special thanks to Mr. Saikat Das, a doctoral student in structural engineering who has also been very supportive throughout my dissertation work. Lastly I would also like to thank the non-academic staff who have contributed towards the completion of my dissertation work.

Date: Lubwama Daudi

Place: Roorkee 17523012

ABSTRACT

Jarosite is generated as a byproduct during the process of zinc extraction from its ore. It is highly toxic in nature and a source of environmental pollution hence its safe disposal is a major concern. The work presented in this dissertation is an experimental account of the tests carried out on concrete in which cement has been replaced by jarosite at percentages of 0%, 15% and 25% to explore its utilisation potential as a construction material.

Isothermal calorimetry has been used to investigate the effect of jarosite on the hydration of cement as well as characterisation of cement paste containing jarosite through X-ray diffraction (XRD) analysis, thermal gravimetric analysis (TGA) and measurement of pH. The performance of concrete containing jarosite has also been assessed in terms of permeability, acid attack, sulphate attack, accelerated corrosion, marine application as well as conducting elevated temperature studies focused on the compressive strength, modulus of elasticity and the stress-strain response.

CONTENTS

LIST OF FIGURES

LIST OF TABLES

CHAPTER ONE

INTRODUCTION

1.1 General

The growth of industrialization in many countries has led to accumulation of industrial wastes in huge quantities which in turn has resulted into development of waste management solutions. The wastes can be hazardous or non-hazardous consisting of organic and/or inorganic materials. Jarosite is an example of an industrial by-product generated during the process of hydrometallurgical zinc extraction.

Figure 1: A sample of jarosite

1.2 Jarosite formation

Metallic zinc extraction process is mainly of (a) goethite process (FeOOH), (b) jarosite process ($XFe_3(SO_4)_2(OH_6)$) and Hematite process and each process has its own advantages and disadvantages [1].

The formation of jarosite and its equilibrium condition is as follows [1]:

$$3Fe_2(SO_4)_3 + X_2SO_4 + 12H_2O \longrightarrow 2XFe_3(SO_4)_2(OH)_6 + 6H_2SO_4 \quad \text{---------- (i)}$$

where X represents H_3O^+, Na^+, K^+, NH_4^+, Ag^+, Li, or 1/2 Pb^{2+}.

In the jarosite process, an Fe (3+) compound of the type X $[Fe_3(SO_4)_2(OH)_6]$ is precipitated by adding alkali metal or ammonium ions [1].

1.3 Toxicity

The toxicity in jarosite is mainly due to the presence of different metals which include; lead, cadmium, arsenic, chromium, zinc, nickel, copper, iron etc. which pollute the soil and ground water [1,2]. The jarosite released during the process can either be recycled for further processing or sent for safe disposal but the quantities of the material generated have made safe disposal without affecting the environment a challenge.

1.4 Objectives

The objectives of the study are:-

1. To understand the effect of jarosite in the process of hydration of cement.
2. To check suitability of jarosite as construction material basing on properties of jarosite-cement paste.
3. To understand the long term performance of concrete containing jarosite.
4. To understand the performance of concrete containing jarosite after exposure to elevated temperature.

CHAPTER TWO

LITERATURE REVIEW

2.1 Jarosite characteristics and its utilisation potentials

Jarosite was characterized according to different parameters as shown in Table 1. Jarosite was then mixed with sand in different mix ratios to form bricks. The bricks were dried, fired and then their engineering properties were tested to determine the mix which could give properties which conform to the quality standards. According to the experimental trials, a mix ratio of 3:1 (jarosite-sand) showed the best properties in terms of density, water absorption and compressive strength which were 1.51 gm/cm^3, 17.46% and 43.4 kg/cm^2 respectively [1].

Table 1: Physico-chemical properties of jarosite [1].

Parameters	**Jarosite**
Sand (%)	4.18
Silt (%)	63.48
Clay (%)	32.35
Texture	Silty clay loam
Bulk density (gm/cc)	0.984
Specific gravity	2.92
Porosity (%)	67.00
Water holding capacity (%)	109.96
Hydraulic conductivity (m/day)	0.037
pH	6.78
Electrical conductivity (dS/m)	13.597

2.2 Solidification- Stabilization Technique for Metal bearing Solid Waste from Zinc Industry –A case study

Jarosite was solidified with different combinations of binder-waste ratio in cement concrete blocks mixed in the ratio of 1:2:4. Fine aggregate was replaced by jarosite in the percentages of; 20%, 40%, 60%, 80% and 100%. Ordinary Portland Cement (OPC), Sulphate Resistant Portland

Cement (SRPC) and their combinations were used as binders. The concrete blocks prepared were tested for compressive strength and toxicity characteristic leaching procedure (TCLP) after 28 days. The results showed that concrete with 40% OPC and 60% SRPC and 60% replacement of fine aggregate by jarosite was the most optimum combination. The leaching tests conducted indicated that Solidification and stabilization technique was effective in terms of restraining of leaching of heavy metals [3].

Table 2: Compressive strength of concrete mixes using OPC and SRPC as binder [3].

Sr. No	Cement		Fine aggregate		Course aggregate (Kg)	Total Weight (Kg)	UCS (28 days curing) in Kg/cm^2	Compressive strength in Kg/cm^2
	SRPC (Kg)	OPC (Kg)	Sand (Kg)	Jarosite (Kg)				
1	0.6	0.4	2.00	0.00	4.0	7.0	170	100
2	0.6	0.4	1.60	0.40	4.0	7.0	160	94.12
3	0.6	0.4	1.20	0.80	4.0	7.0	155	91.76
4	0.6	0.4	0.80	1.20	4.0	7.0	150	88.24
5	0.6	0.4	0.40	1.60	4.0	7.0	120	70.59
6	0.6	0.4	0.00	2.00	4.0	7.0	80	47.06

2.3 Properties of concrete containing jarosite as a partial substitute for fine aggregate

Here properties of concrete in which jarosite was used a partial substitute for fine aggregate at different w/c ratios along with fly ash were investigated. The results obtained showed that addition of jarosite to the concrete improved the compressive strength and flexural strength. The water permeability and abrasion were also found to be within the acceptable standards as well as the toxicity leaching characteristics. Concrete mixtures with w/c 0.45 turned out to be more suitable for jarosite addition than other water-cement ratios. The mix design proportions for the experimental trials of the study are presented in Table 3 [4].

Table 3: Mixture proportions of fresh concrete [4].

FA replacement %	Water-cement ratio	Water (kg)	Cement (kg)	Fly ash (Kg)	Fine aggregate (Kg)	10 mm (kg)	20 mm (kg)	Jarosite (Kg)	Admixture (gm)	Compacting factor
0	0.40	15.2	28.5	9.5	71.300	58.2	58.2	0	304	0.96
5	0.40	15.2	28.5	9.5	67.735	58.2	58.2	3.565	342	0.97
10	0.40	15.2	28.5	9.5	64.170	58.2	58.2	7.130	418	0.97
15	0.40	15.2	28.5	9.5	60.605	58.2	58.2	10.695	494	0.98
20	0.40	15.2	28.5	9.5	57.040	58.2	58.2	14.260	570	0.98
25	0.40	15.2	28.5	9.5	53.475	58.2	58.2	17.825	646	0.96
0	0.45	17.1	28.5	9.5	71.300	58.2	58.2	0	152	0.97
5	0.45	17.1	28.5	9.5	67.735	58.2	58.2	3.565	228	0.99
10	0.45	17.1	28.5	9.5	64.170	58.2	58.2	7.130	304	0.98
15	0.45	17.1	28.5	9.5	60.605	58.2	58.2	10.695	380	0.97
20	0.45	17.1	28.5	9.5	57.040	58.2	58.2	14.260	494	0.97
25	0.45	17.1	28.5	9.5	53.475	58.2	58.2	17.825	570	0.98
0	0.50	19.0	28.5	9.5	71.300	58.2	58.2	0	0	0.96
5	0.50	19.0	28.5	9.5	67.735	58.2	58.2	3.565	114	0.97
10	0.50	19.0	28.5	9.5	64.170	58.2	58.2	7.130	190	0.96
15	0.50	19.0	28.5	9.5	60.605	58.2	58.2	10.695	228	0.95
20	0.50	19.0	28.5	9.5	57.040	58.2	58.2	14.260	304	0.97
25	0.50	19.0	28.5	9.5	53.475	58.2	58.2	17.825	380	0.98

2.4 Characterization, leachate Characteristics and compressive strength of Jarosite/clay/fly ash bricks

Jarosite was mixed with clay in four different ratios; 1:1, 1:2, 1:3 and 1:4 with fly ash as shown in Table 4. Each of these ratios was mixed together with 0%, 5%, 10%, 15% and 20% of fly ash each to give a total mass of 100kg to make bricks. The bricks were sun-dried and then fired in the furnace at 900ºC for an hour. Experimental trials revealed that mix ratios of 1:1 and 2:1 of jarosite and clay along with 15% and 20% of fly ash produced sintered clay bricks with acceptable compressive strength [2].

Table 4: Mix design used for sample preparation [2].

Jarosite:Clay	Jarosite (g)	Clay (g)	Fly ash (g)	Total mass (g)
1:1	50	50	0	100
1:1	47.5	47.5	5	100
1:1	45	45	10	100
1:1	42.5	42.5	15	100
1:1	40	40	20	100
2:1	66.7	33.3	0	100
2:1	63.3	31.7	5	100
2:1	60	30	10	100
2:1	56.7	28.3	15	100
2:1	53.3	26.7	20	100
3:1	75	25	0	100
3:1	71.3	23.8	5	100
3:1	67.5	22.5	10	100
3:1	63.8	21.25	15	100
3:1	60	20	20	100
4:1	80	20	0	100
4:1	76	19	5	100
4:1	72	18	10	100
4:1	68	17	15	100
4:1	64	16	20	100

CHAPTER THREE

EXPERIMENTAL WORK

3.1 Hydration studies

An isothermal calorimetric experiment has been carried to investigate the effect of jarosite on the process of hydration of cement (OPC and PPC) using a I-Cal 4000 HPC Isothermal Calorimeter. 100 ml of water is filled in cups which are placed into a high precision calorimeter for 24 hours to attain an isothermal condition. Four samples of OPC each 40 grams mixed with different percentages of jarosite which include; 0%, 10%, 15% and 25% were prepared as shown in Figure 2 below where 0% composition of jarosite was used as a control for the experiment.

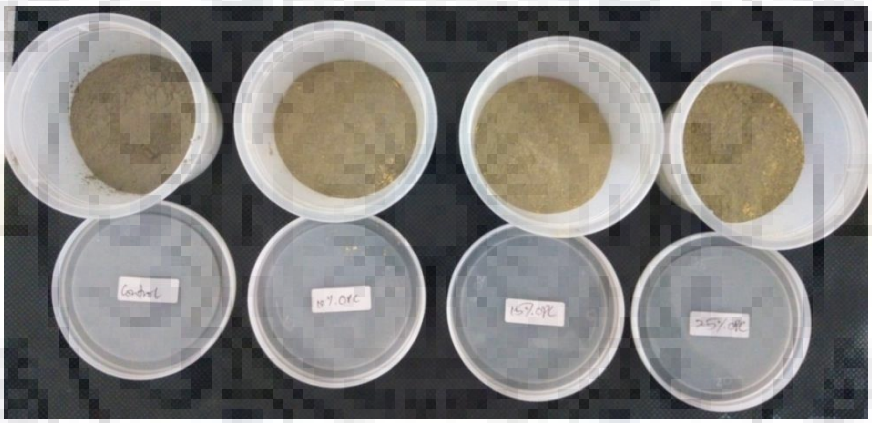

Figure 2: Samples of OPC with jarosite compositions; 0%, 10%, 15% and 25%

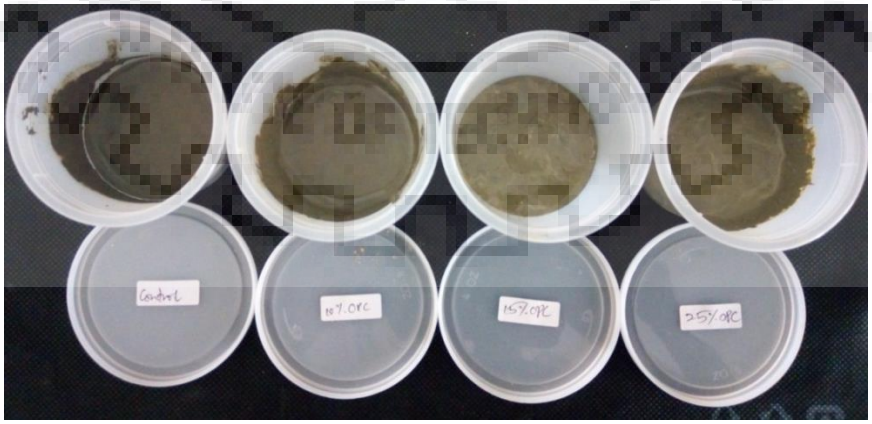

Figure 3: Samples of OPC with jarosite after mixing each with 20ml of water

Each sample was mixed with 20 ml of the water from the calorimeter after attaining isothermal condition as shown in Figure 3 and then placed in the calorimeter for 72 hours as the process of hydration for each sample was monitored. A plot showing the rate of heat release as a function of time obtained from the experiment is presented in Figure 32. A similar experiment has been carried with PPC samples prepared the same way as described for OPC and the plot showing the rate of heat release as a function of time is presented in Figure 33.

3.2 X-Ray diffraction (XRD) analysis

Jarosite was mixed with cement in doses of 0%, 15% and 25% together with water added according to their respective consistencies to make pellets of the respective jarosite compositions for both OPC and PPC. The pellets were then kept in water for hydration to take place for 28 days. After 28 days, the pellets were kept in ethanol for 7 days to stop hydration after which they were oven-dried as shown in Figure 4 and Figure 5 then finely ground to obtain powdered samples for both OPC and PPC with jarosite percentage compositions of 0%, 15% and 25% as shown in Figure 7 and Figure 8.

X-ray diffraction analysis has been carried out on the finely ground powdered samples using the Bruker AXS diffraktometer D8 ADVANCE machine in Figure 9 and x-ray diffraction patterns of the samples are shown in Figure 43 and Figure 44.

Figure 4: Dry pellets of OPC with jarosite compositions of 0%, 15% and 25% before grinding

Figure 5: Dry pellets of PPC with jarosite compositions of 0%, 15% and 25% before grinding

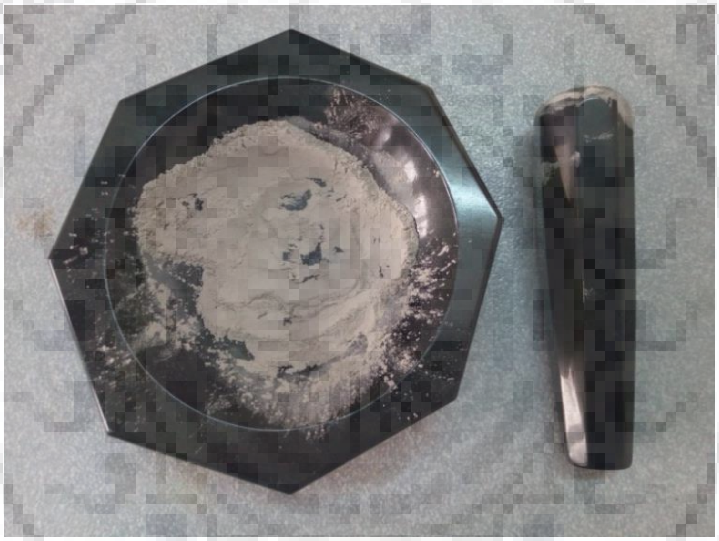

Figure 6: Sample preparation of one of the powdered samples for XRD analysis

Figure 7: Samples of OPC with jarosite compositions of 0%, 15% and 25% for XRD analysis

Figure 8: Samples of PPC with jarosite compositions of 0%, 15% and 25% for XRD analysis

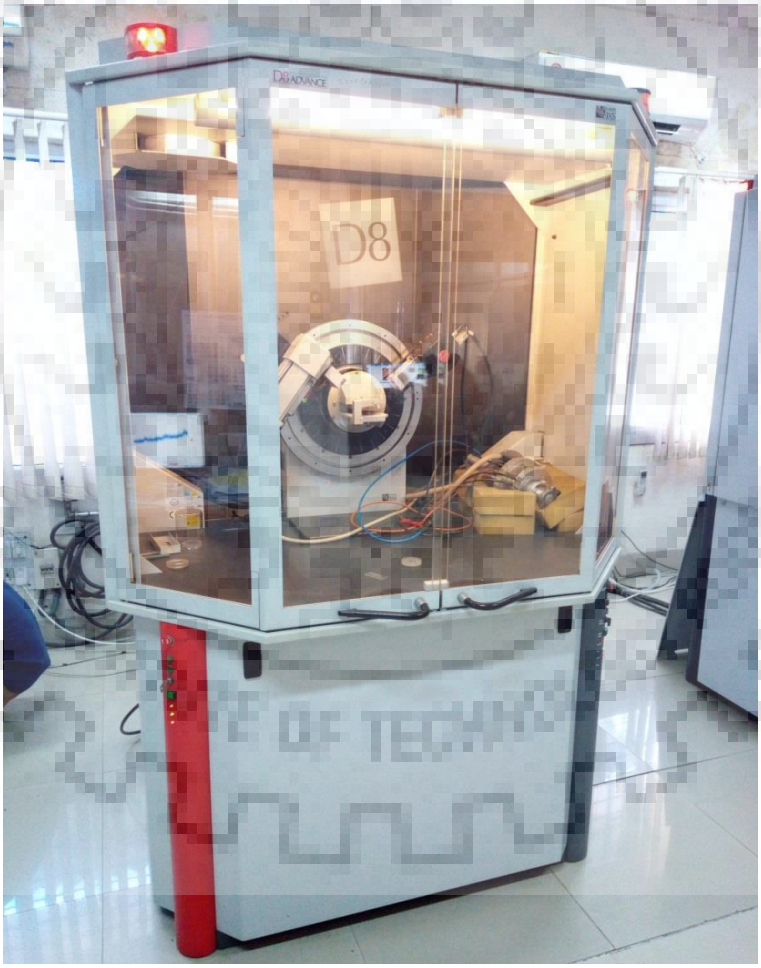

Figure 9: The Bruker AXS diffraktometer D8 ADVANCE machine used for the XRD analysis

3.3 Thermal gravimetric analysis (TGA)

Thermal gravimetric analysis has been carried out on finely ground powdered samples of both OPC and PPC with jarosite percentage compositions of 0%, 15% and 25% prepared the same way described above for XRD samples. The powdered samples have been heated from ambient temperature up to 1000ºC at a heating rate of 10 ºC per minute in a nitrogen atmosphere using the EXSTAR TG/DTA 6300 machine in Figure 10. The TGA and DTA curves for OPC samples are presented in Figure 45 and Figure 46 while TGA and DTA curves for PPC samples are shown in Figure 47 and Figure 48 respectively.

Figure 10: The EXSTAR TG/DTA 6300 machine used for the Thermal gravimetric analysis

3.4 Measurement of the pH

Finely ground powdered samples were obtained from concrete containing jarosite with percentage compositions of 0%, 15% and 25% for both OPC and PPC. 2 grams of each powered sample is mixed with 100 ml of distilled water and stirred to dissolve into a uniform solution.

After stirring, the pH electrode of the pH meter is dipped into the solution until a constant pH value was displayed by pH meter as shown in Figure 11 below. Table 6 shows the pH values for every sample as measured by the pH meter.

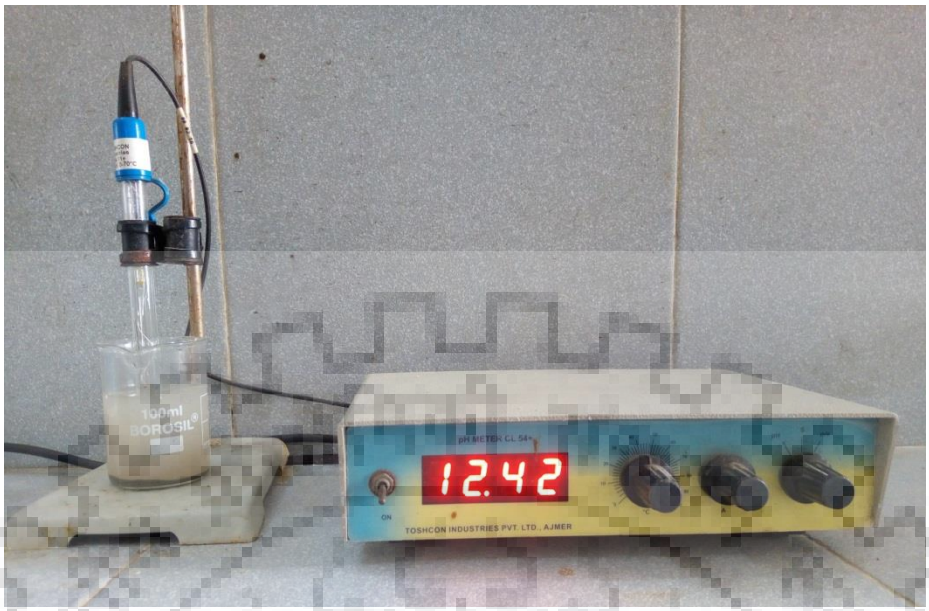

Figure 11: pH measurement of a 0% OPC powdered sample in solution using a pH meter

3.5 Permeability

An experiment has been carried out to evaluate the water permeability of concrete containing jarosite described as follows. Six cylindrical specimens of 150 mm diameter and 300 mm height were cast and then each cut into two to obtain twelve specimens of 150 mm diameter and 150 mm height. The specimens have percentage compositions of 0%, 15% and 25% of jarosite by replacement of both OPC and PPC which included two specimens of each. Epoxy coating has been applied on the sides of each of the specimens to prevent the water from escaping from the sides of the specimens by evaporation during the testing.

Three specimens have been placed in the testing machine (in Figure 13) at the same time and each exposed to water under a pressure of 10kg/cm^2 on the top surface for 100 hours. At the end of the test period, the specimens are split open as shown in Figure 14 and the depth of penetration measured. The results for both OPC specimens and PPC specimens are shown in Table 9. The results of coefficient of permeability in Table 10 and Table 11 have been determined according to the formula below:

$$K_p = \frac{d^2 \nu}{2Th}$$

Where; *Kp* = coefficient of permeability in m/sec, *d* = depth of penetration in metres, *T* = time to penetrate depth *d* in seconds, *h* = pressure head in metres, *v* = porosity of the concrete in fraction.

Figure 12: The permeability testing machine

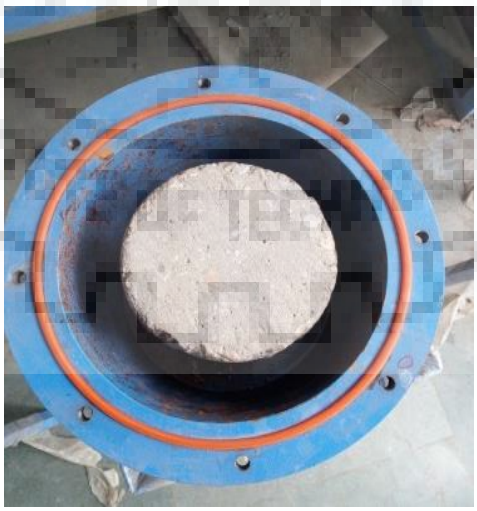

Figure 13: One of the specimens fitted into the test cell before testing

Figure 14: Splitting one of the specimens at the end of the test period

Figure 15: One of the specimens split into two at the end of the test period

3.6 Acid attack

For determining the effect of acid attack on jarosite based concrete, concrete cubes of both OPC and PPC with jarosite compositions of 0%, 15% and 25% have been considered. Six cubes of 10 cm in size for each percentage composition were cast of which three cubes were used as control specimens while the other three were immersed in 2.5% (by volume) solution of sulphuric acid as shown in Figure 16 for 28 days. After the 28 days of immersion the cubes are taken out of the acid solution, dried, weighed and the compressive strength was tested as seen in Figure 19. The percentage loss in mass and compressive strength have been determined and the results of OPC specimens are provided in Table 12 and Table 13 respectively while the results for PPC specimens are provided in Table 14 and Table 15.

Figure 16: Specimens of 0% OPC and 0% PPC immersed in 2.5% solution of sulphuric acid

Figure 17: Dried specimens of 0% OPC after acid attack

Figure 18: Dried specimens of 25% OPC after acid attack

Figure 19: Testing one of the dried specimens of 0% OPC after acid attack

3.7 Sulphate attack

For determining the effect of sulphate attack on jarosite based concrete, concrete cubes of both OPC and PPC with jarosite compositions of 0%, 15% and 25% have been considered. Six cubes of 10 cm in size for each percentage composition were cast of which three cubes were used as control specimens while the other three were immersed in 7% (by weight) solution of sodium sulphate as seen in Figure 20 for 28 days. After the 28 days of immersion the cubes are taken out of the solution, dried and the compressive strength is tested as shown in Figure 21. The percentage loss in compressive strength has been determined for both OPC and OPC as provided in Table 16 and Table 17 respectively.

Figure 20: Specimens of 0% OPC and 0% PPC immersed in 7% solution of sodium sulphate

Figure 21: Testing one of the dried specimens of 0% OPC after sulphate attack

3.8 Corrosion

An experiment has been carried out to evaluate the corrosion of steel in concrete containing jarosite by measuring the loss in weight of steel at the end of the test. The experiment involves partial immersion of concrete cylinders of diameter 150 mm and 300 mm with a bar of 12 mm diameter at the centre into a 5% solution of sodium chloride as shown in Figure 23. The cylinders are of 0%, 15% and 25% replacement of cement by jarosite.

The steel bar in each specimen has been connected to the positive terminal of the DC supply machine and the steel plates are connected to a negative terminal (Figure 22). A current of 0.11 ampere has been passed through the bar of each specimen for 20 days. After the 20 days, the bars are extracted from each of the specimens as shown in Figure 24 and Figure 25 then cleaned and weighed to determine the mass loss.

The experiment has been carried out with specimens of both OPC as well as PPC and the results are shown in Table 18 and Table 19 respectively. After fixing the corrosion time, current has been determined as per the following expression:

$$t = \frac{mnC}{IM}$$

Where: t = time in seconds, m = mass loss in gram, C = Faraday's constant, I = current in ampere, M = molar mass

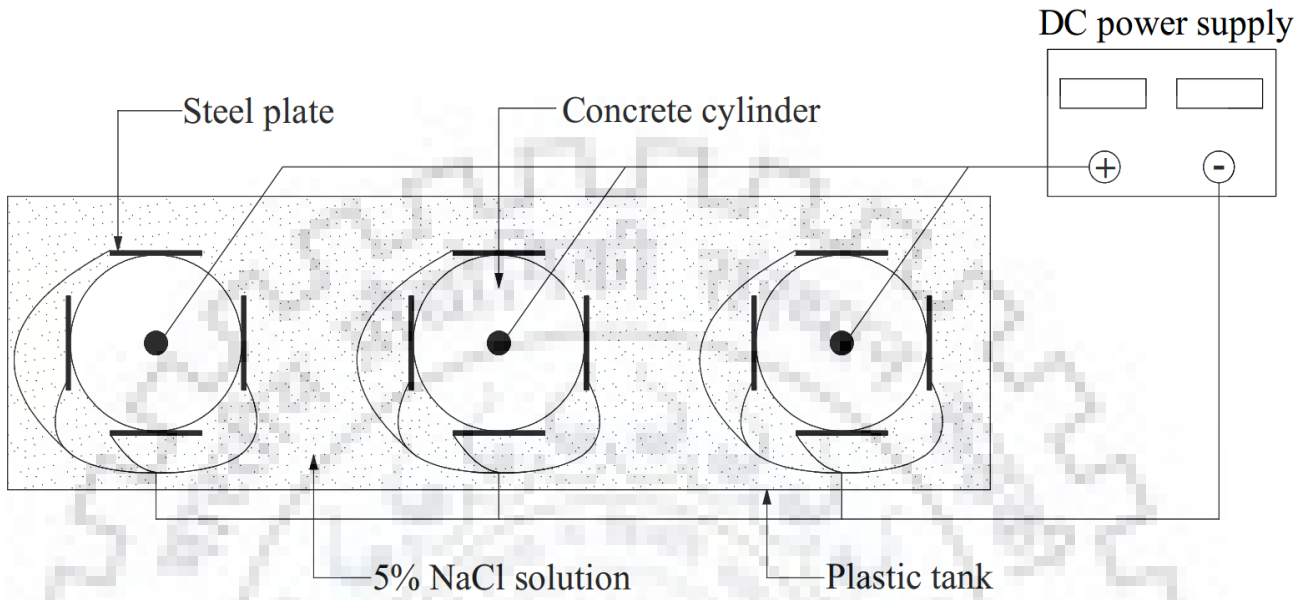

Figure 22: A schematic diagram of three specimens connected in a circuit for the corrosion test

Figure 23: Specimens immersed in 5% sodium chloride solution

Figure 24: Bars extracted from of the specimens of 0% PPC and 25% PPC after 20 days

Figure 25: Bars extracted from of the specimens of 15% OPC and 15% PPC after 20 days

3.9 Marine application

An experiment has been carried out to investigate the chloride penetration in concrete containing jarosite which was exposed to wetting and drying cycles to simulate marine conditions. Cubes of 10cm were cast and cured for 28 days. Epoxy coating is applied on five faces leaving one face open to allow unidirectional chloride ingression and then immersed in a 1.0M NaCl solution. The cubes are subjected to six hours of wetting and eighteen hours of drying per day and this is done for 21 cycles.

After 21 cycles, samples are obtained by grinding at depths of 0 mm, 5 mm, 10 mm, 15 mm, 20 mm and 25 mm from the open surface (Figure 26 (a)). The chloride content in each of the samples obtained has been determined using Nordtest method (NT BUILD 208). About 5 gm of sample has been taken in a glass bottle from each sample and it is oven dried for 2 hours then cooled in a dessicator.

20 ml distilled water, 10 ml concentrated nitric acid and 50 ml boiling hot distilled water has been added and shaken properly then the mixture is allowed to cool for one hour. After one hour cooling, the solution is filtered. Rinsing of filter has been done twice with 1% nitric acid solution. 10ml of 0.1N silver nitrate solution, 2-3 ml benzyl alcohol and 1ml saturated ammonium ferrisulphate solution has been added in the filtered solution.

After all this, titration has been done with 0.1N ammonium thiocyanate solution until the solution attained a weakly red colour (Figure 26 (b)). The chloride content is obtained according to the following expression:

$$\text{Weight } \%Cl^- = \frac{3.545(V_1N_1 - V_2N_2)}{m}$$

Where: V_1 = added amount of silver nitrate solution (ml), N_1 = normality of silver nitrate solution, V_2 = added amount of ammonium thiocyanate solution (ml), N_2 = normality of ammonium thiocyanate solution, m = weight of sample (gm). The results are tabulated in Table 20 for which a graph of chloride content versus depth has been plotted in Figure 53.

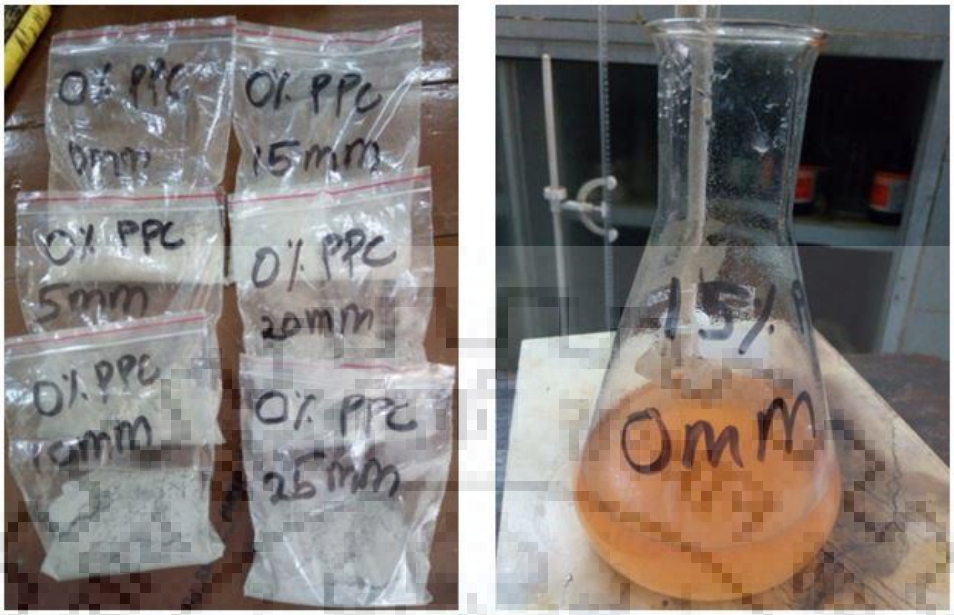

(a) (b)

Figure 26: (a) Samples obtained from a specimen of 0% PPC. (b) One of the samples after reaching the titration endpoint.

3.10 Elevated temperature studies

Mix design has been done in accordance with IS 10262 for M25 grade of concrete with both OPC and PPC using a water-cement ratio of 0.5. The quantities of ingredients of the design mix in Kg per cubic metre are presented in Table 5.

Table 5: Quantity of mix design ingredients (Kg/m^3)

Cement	Fine aggregate	Course aggregate	water
372	675	1175	186

Cylindrical specimens of diameter 150 mm and 300 mm height with jarosite compositions of 0%, 15% and 25% were cast into cylindrical moulds and vibrated on a vibrating table. After 24 hours, demoulding was done and the specimens were placed in a curing tank for 28 days. After 28 days of curing, the specimens were retrieved from the curing tank then their top surfaces grinded to make them smooth and levelled. For each of the jarosite compositions considered, one specimen was cast with three thermocouples were provided inside at heights of 50 mm, 150 mm and 250 mm.

Such specimens were used to monitor the temperature of the specimen in the furnace in order to establish the time taken for specimens of a particular jarosite composition to reach the target temperature.

Figure 27: Grinding one of the samples after 28 days of curing

Figure 28: Some of the cylindrical specimens after grinding the top surface

Three specimens of each jarosite composition have been heated up to 350ºC and 600ºC at a rate of 0.5ºC per minute in an electric furnace. After reaching the target temperature, the specimen is left in the furnace for four hours to attain a homogenous thermal state. Thereafter the furnace is switched off and the sample is left inside to cool down gradually. The residual mechanical properties which include compressive strength, stress-strain response and the modulus of elasticity have been investigated.

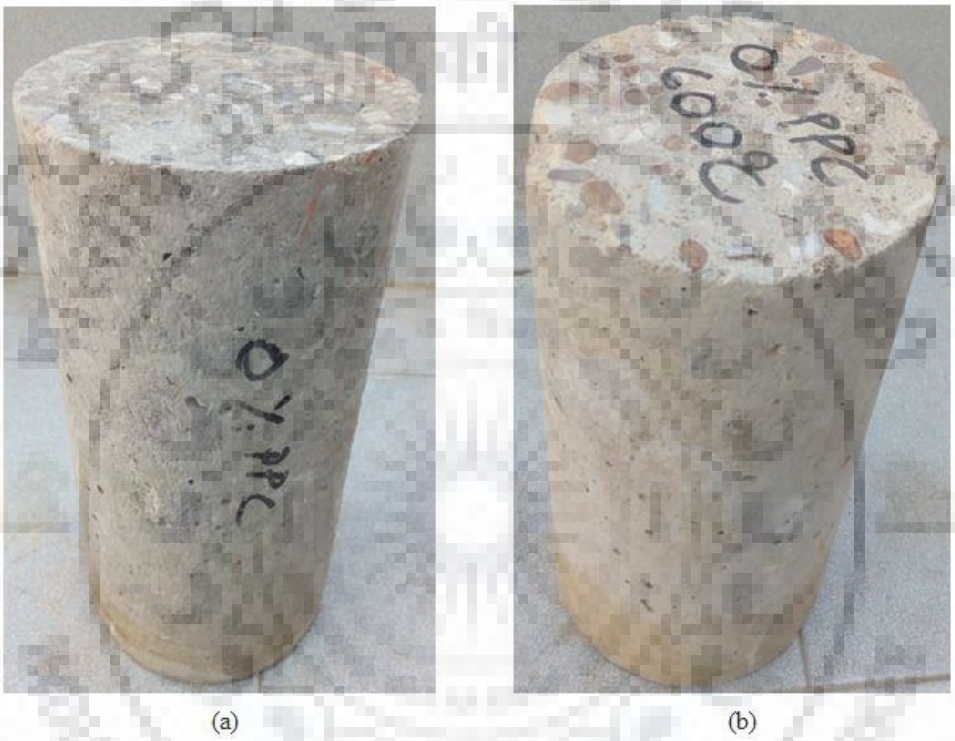

Figure 29: (a) 0% PPC specimen before heating. (b) 0% PPC specimen after heating to 600ºC.

3.11 Compressive strength tests and stress-strain response

Compressive strength tests for all the specimens considered have been done after 28 days of curing under three different conditions; ambient temperature, exposure to 350ºC and 600ºC. All the heated specimens have been tested after gradually cooling to ambient temperature and therefore the compression test results correspond to the residual compressive strength and not high temperature compressive strength. The stress-strain relationships for the respective specimens have been obtained concurrently during the compressive strength tests under displacement control.

Figure 30: Testing 15% PPC control specimen

3.12 Modulus of Elasticity

The modulus of elasticity for all the specimens considered has been tested after 28 days of curing under three different conditions; ambient temperature, exposure to 350ºC and 600ºC in accordance to ASTM C469/C469M-14. Here specimens have been exposed to cyclic loading of twelve cycles in which six cycles for a quarter of the peak load and the other six cycles of half the peak load. This was done in order to keep the concrete in the elastic zone without reaching the elastic limit. For each cycle, the values of Young's modulus (the slope) were recorded. Nine values were obtained for each specimen and the average value was taken to be the modulus of elasticity for a particular specimen.

However, this was not possible for specimens exposed to 600ºC because of the low values of their peak load. For the case of such specimens, the slope of the straight segment between the origin and the peak stress has been obtained from their stress-strain graphs to be taken as their modulus of elasticity.

Figure 31: Testing for the modulus of elasticity of 25% PPC control specimen

CHAPTER FOUR

RESULTS AND DISCUSSION

4.1 Hydration of cement mixed with jarosite

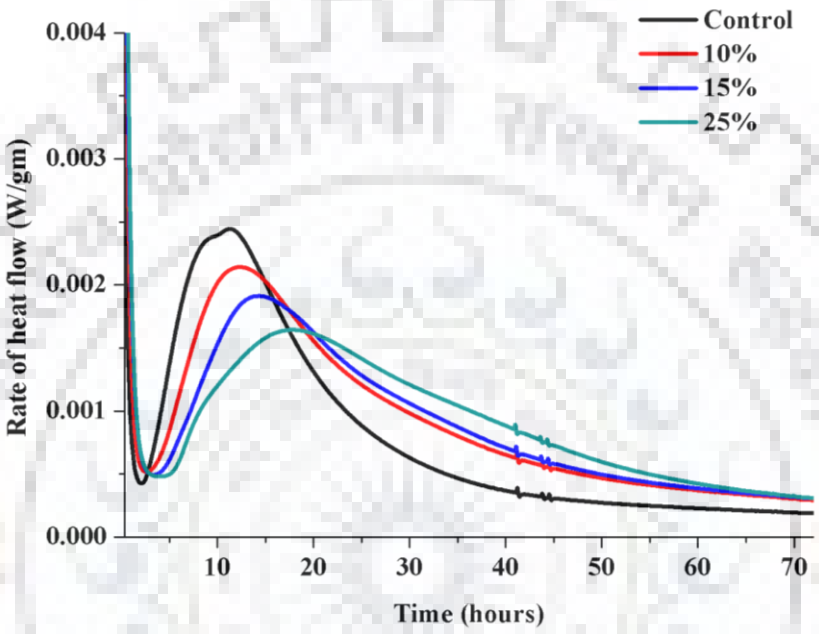

Figure 32: A plot showing the rate of heat release as a function of time for OPC

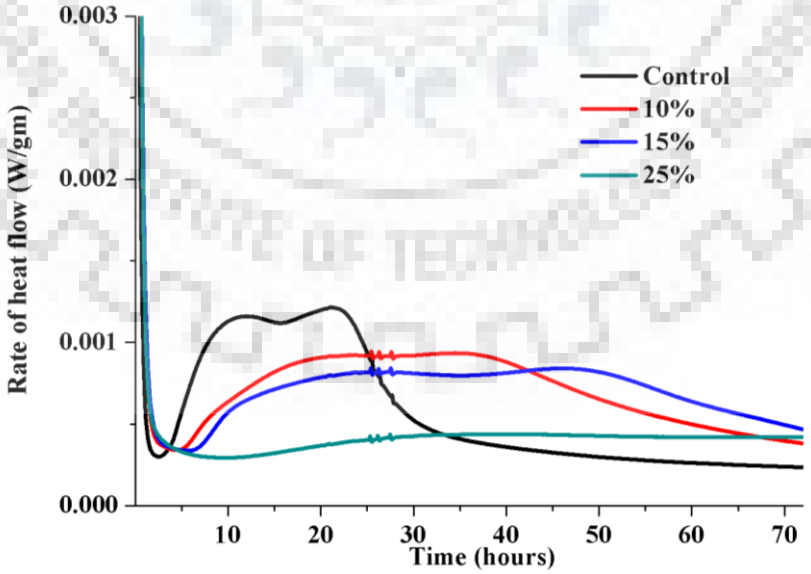

Figure 33: A plot showing the rate of heat release as a function of time for PPC

From the Figure 32, it can be observed that the period for the initial reaction increases as the jarosite composition increases in the samples i.e. control < 10% OPC < 15% OPC < 25% OPC and also a similar behaviour is shown by PPC samples in Figure 33.

This is attributed to the presence of a substantial amount of SO_3 in jarosite which leads to the release of SO_4^{2-} ions into solution when jarosite is dissolved in water. These react with C_3A in the cement to form ettringite which creates a barrier around the surfaces of C_3A hence slowing down the reaction by restricting contact with water. Consequently, the whole of the hydration process is retarded. Figure 34 shows the formation of a barrier by ettringite during hydration of C_3A in the presence of SO_4^{2-} ions.

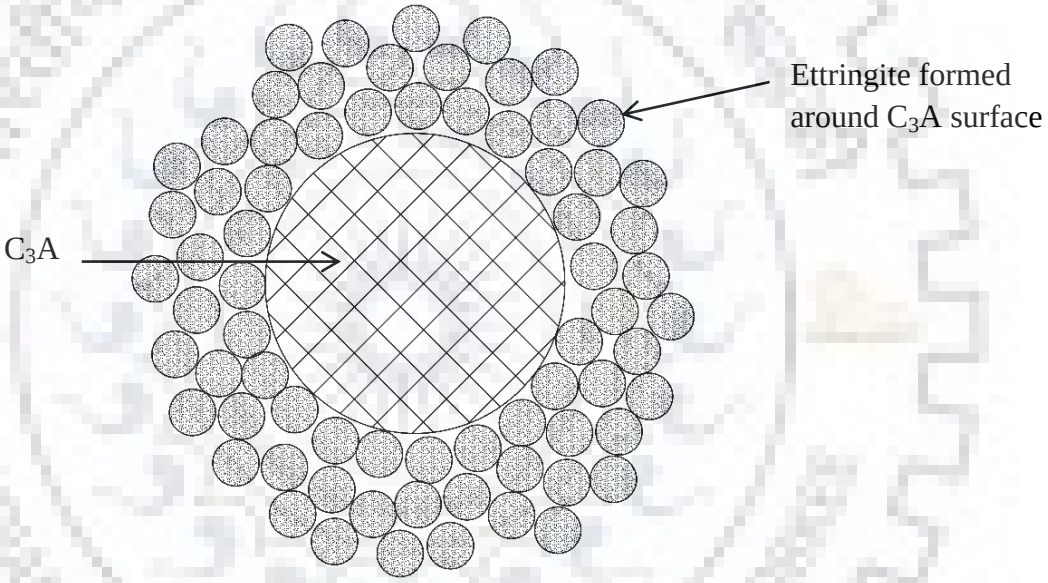

Figure 34: Formation of ettringite around the surface of C_3A during hydration

The grain size distribution also plays a significant role in the hydration process due to jarosite grains being finer than cement grains. As a result, jarosite grains are attached to the surface of cement grains which also creates a barrier around the surfaces of the cement grains thus impeding the diffusion process. This is well illustrated by Figure 35 and Figure 36 presented below in which the former shows the hydration of cement in the control samples while the latter shows the hydration of cement mixed with jarosite.

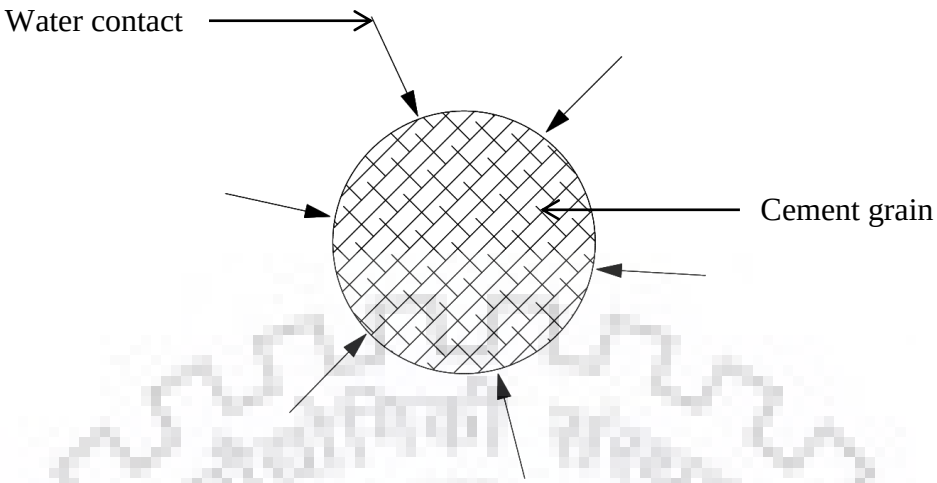

Figure 35: Hydration of cement in control sample

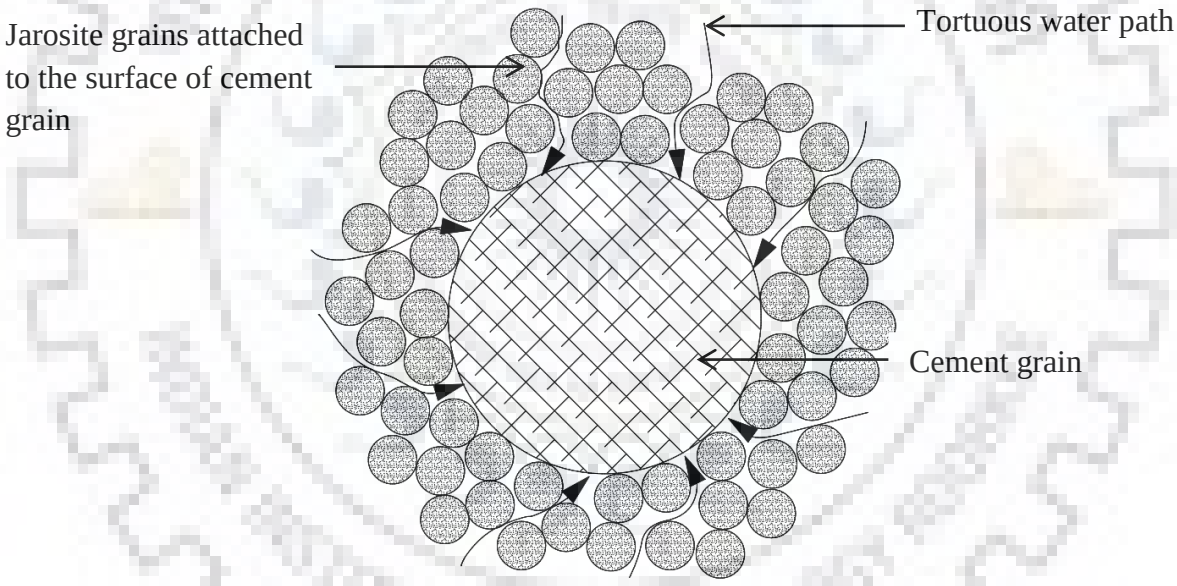

Figure 36: Hydration of cement mixed with jarosite

In relation to the above, consequently the initial reaction takes longer with increase in the jarosite composition which is also followed by a longer induction period in both OPC and PPC. The length of the induction period also follows the order; control < 10% OPC < 15% OPC < 25% OPC as shown in Figure 37 and likewise for PPC samples as shown in Figure 38.

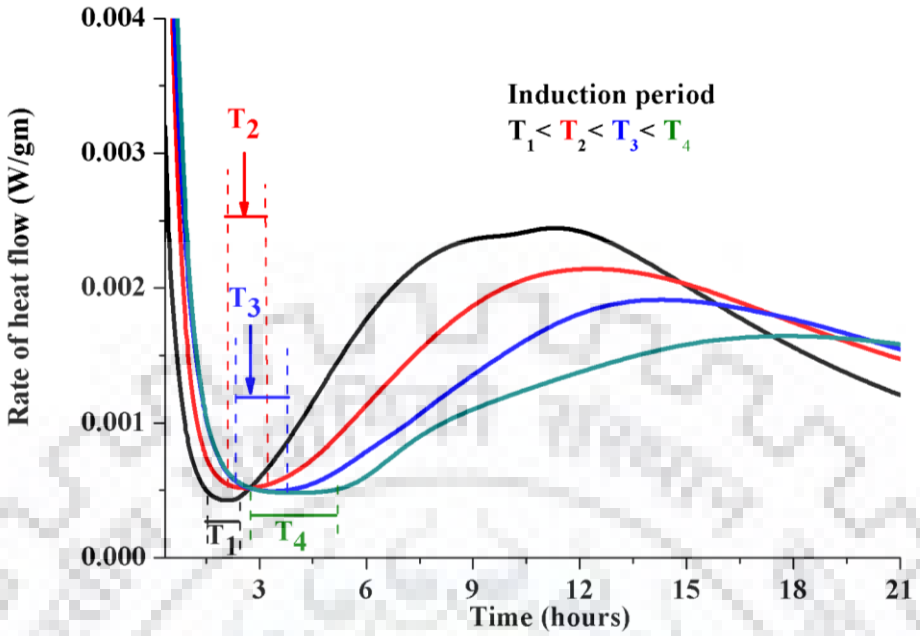

Figure 37: Induction period in OPC

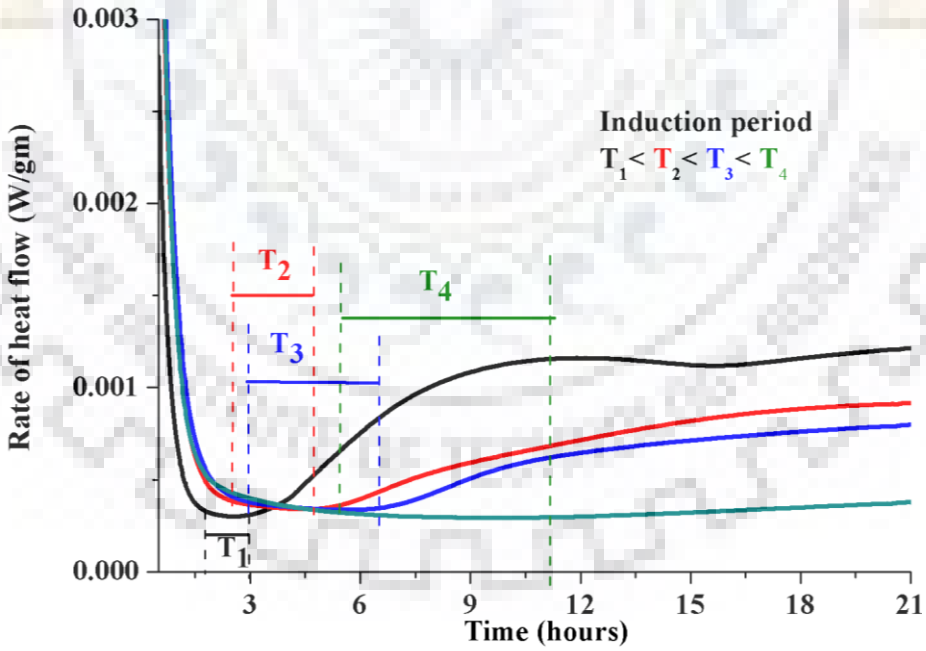

Figure 38: Induction period in PPC

After the induction period, the reaction accelerates due to rapid precipitation of CSH and $Ca(OH)_2$ from hydration of silicates as shown in equation (ii) [5]. However, it can be seen that the acceleration peak becomes lower with increase in the jarosite content i.e. control > 10% OPC > 15% OPC > 25% OPC and similarly for PPC.

$$2(3CaO.SiO_2) + 6H_2O \longrightarrow 3CaO.2SiO_2.3H_2O + 3Ca(OH)_2 \quad \text{---------- (ii)}$$

This is because jarosite does not contain silicates while cement does. Therefore, cement is the only material which contributes silicates in the mix hence reducing the quantity of cement directly reduces the quantity of the silicates available for reaction. Consequently, less quantity of CSH is produced and also a reduction in the heat evolved is observed as the jarosite content increases.

It can also be observed that the acceleration peak in PPC is lower as compared to that in OPC. This is due to the composition of PPC being a combination of Portland cement and a pozzolanic material blended together which also contributes to a slower rate of hydration as compared to OPC [6]. Consequently, the retarding effect of jarosite on the hydration process is exaggerated in PPC as compared to OPC.

The acceleration is followed by a deceleration. The reduction in the rate of reaction is a result of the formation of a thick layer of hydration products around the silicates which creates a barrier for the water thus impeding the diffusion process.

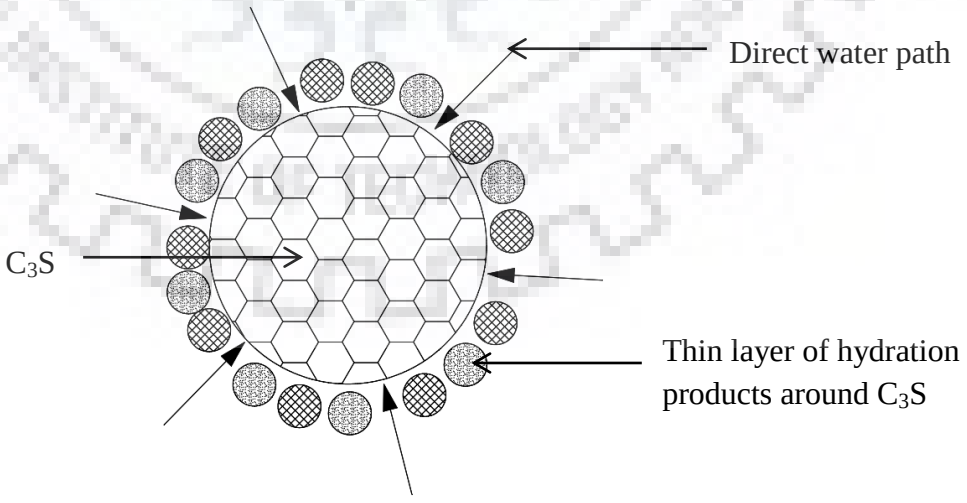

Figure 39: C_3S during the initial stages of hydration

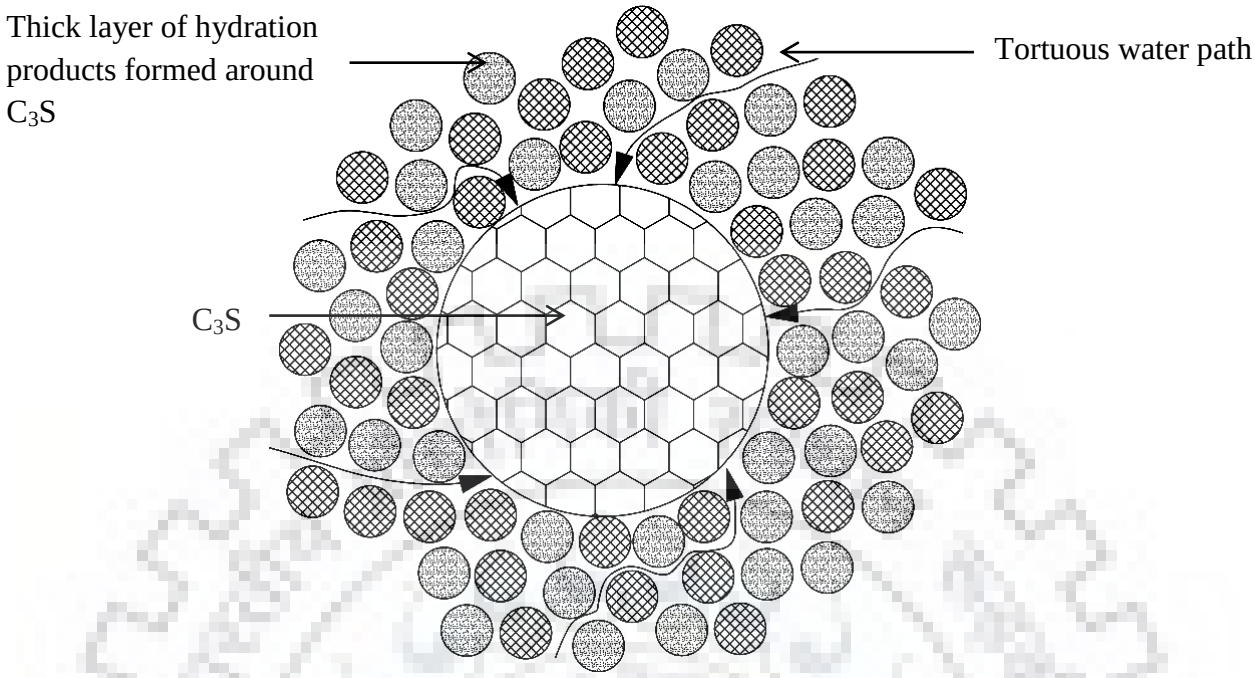

Figure 40: C_3S during the deceleration period

It is also noticeable that more energy is released at later stages of hydration in samples of OPC mixed with jarosite than in the OPC control sample. This is attributed to the pozzolanic reaction between the $Ca(OH)_2$ produced from the primary hydration and the silica (SiO_2) in jarosite as shown in equation (iii) [5].

$$3Ca(OH)_2 + 2SiO_2 + H_2O \longrightarrow 3CaO.2SiO_2.3H_2O \quad \text{---------- (iii)}$$

Unlike PPC, OPC does not contain any pozzolanic material and therefore no pozzolanic reaction happens in the OPC control sample hence less energy is released in the later stages of hydration in the OPC control sample compared to samples of OPC mixed with jarosite.

The effect of the pozzolanic reaction at the later stages of hydration as a result of jarosite addition is also shown in the energy curves presented in Figure 41 and Figure 42 by the increase in the overall energy given out as more jarosite is added to cement. In addition, the overall retarding effect of jarosite on the hydration process is revealed in both OPC and PPC.

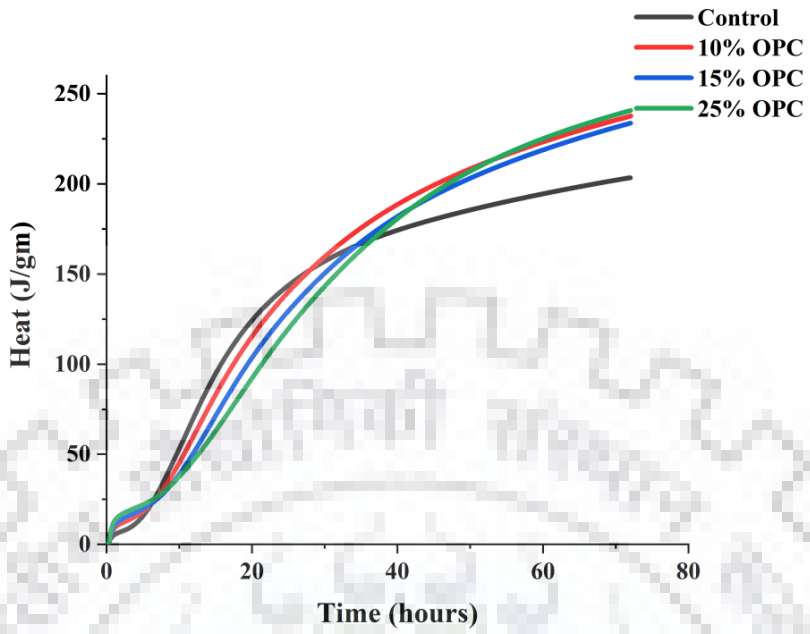

Figure 41: Variation of cumulative energy with time for OPC

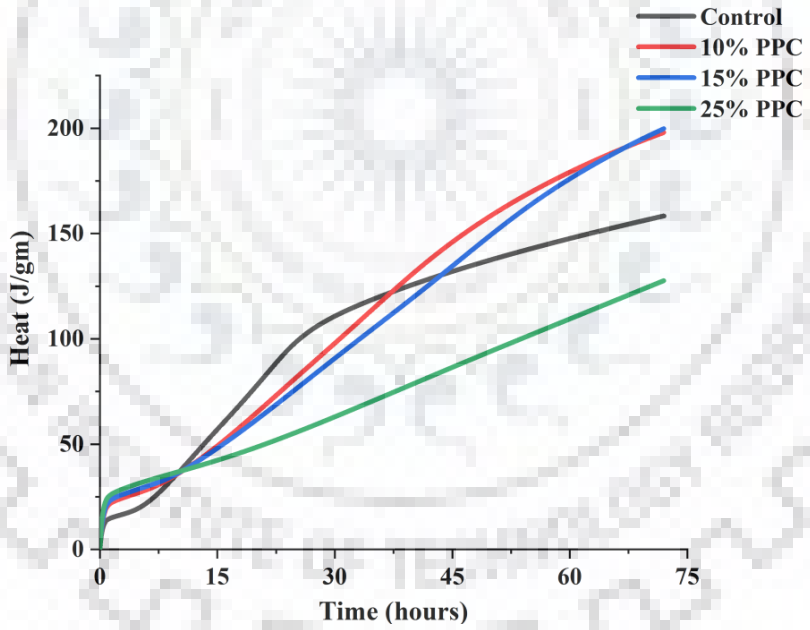

Figure 42: Variation of cumulative energy with time for PPC

The deficiency of the CSH produced when cement is mixed with jarosite due to the reduction in the silicates is compensated by the pozzolanic reaction as per the equation (iii) above. However, at high percentages of jarosite content the deficiency is too much to be compensated by the secondary reaction.

4.2 X-Ray diffraction (XRD) analysis

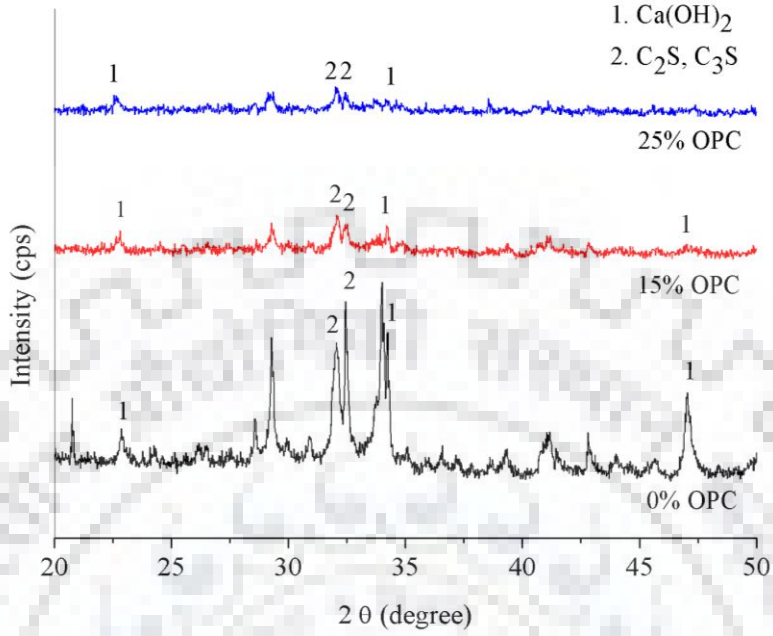

Figure 43: X-ray diffraction patterns of OPC samples

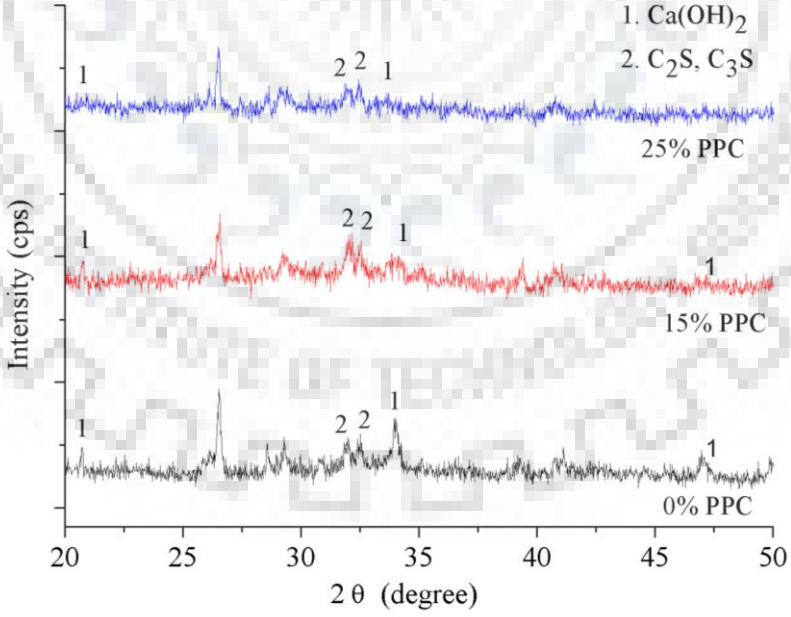

Figure 44: X-ray diffraction patterns of PPC samples

The x-ray diffraction patterns in Figure 43 revealed the presence of crystalline phases of dicalcium silicate (C_2S) and tricalcium silicate (C_3S) together with portlandite ($Ca(OH)_2$) at all jarosite compositions in OPC. However it can also be observed that quantities of the silicates (C_2S and C_3S) and portlandite ($Ca(OH)_2$) decrease as the jarosite composition in OPC increases. The same behaviour is shown by PPC samples in Figure 44.

The reduction in the quantity of silicates i.e. dicalcium silicate (C_2S) and tricalcium silicate (C_3S) is due to the absence of the silicates in jarosite. As explained earlier, cement is the only material in the mix which is responsible for the availability of silicates and hence a reduction in cement content means a reduction in the quantity of silicates available for reaction.

The decrease in portlandite ($Ca(OH)_2$) for both OPC and PPC samples with increase in jarosite content is because jarosite contains silica (SiO_2) which reacts with $Ca(OH)_2$ produced from the primary reaction to produce more calcium silicate hydrate (CSH). As a result, less quantities of $Ca(OH)_2$ are observed in samples with high percentages of jarosite.

4.3 Thermal gravimetric analysis (TGA)

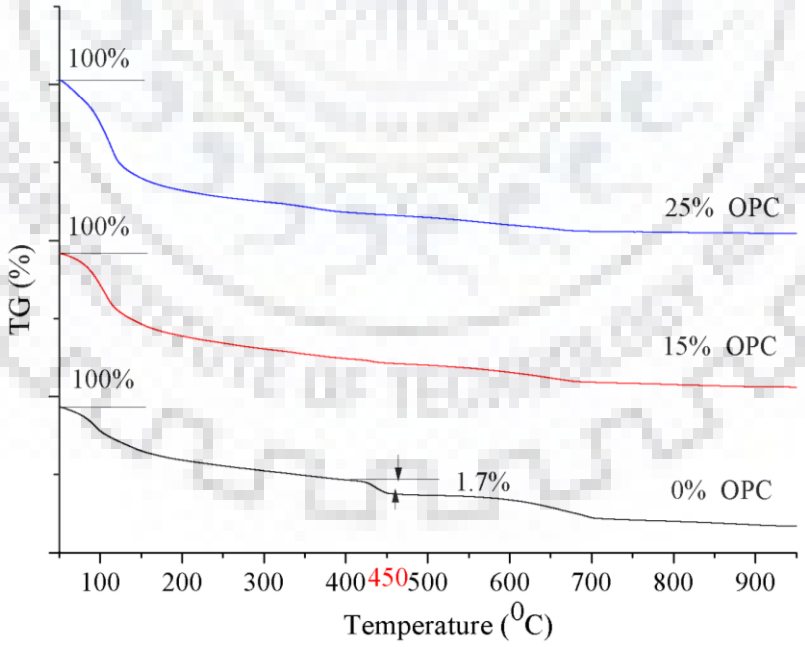

Figure 45: TGA curves of the OPC samples

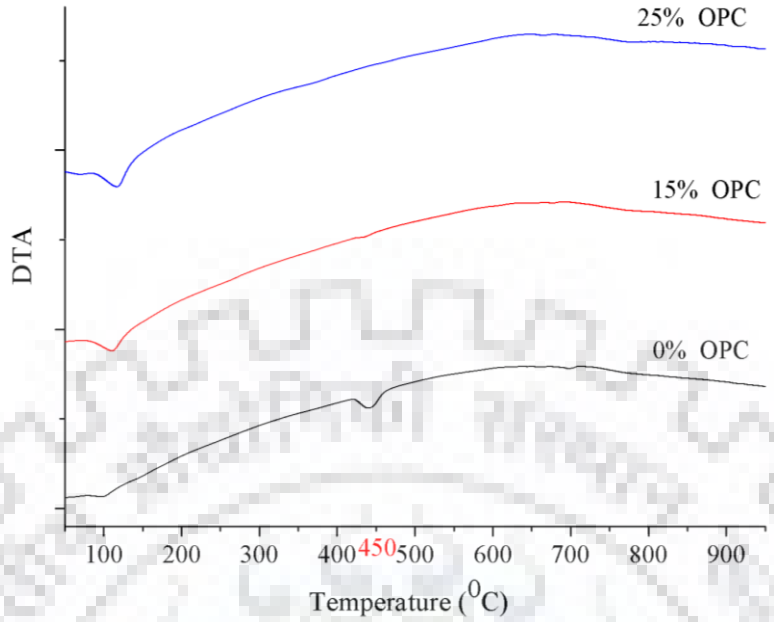

Figure 46: DTA curves for the OPC samples

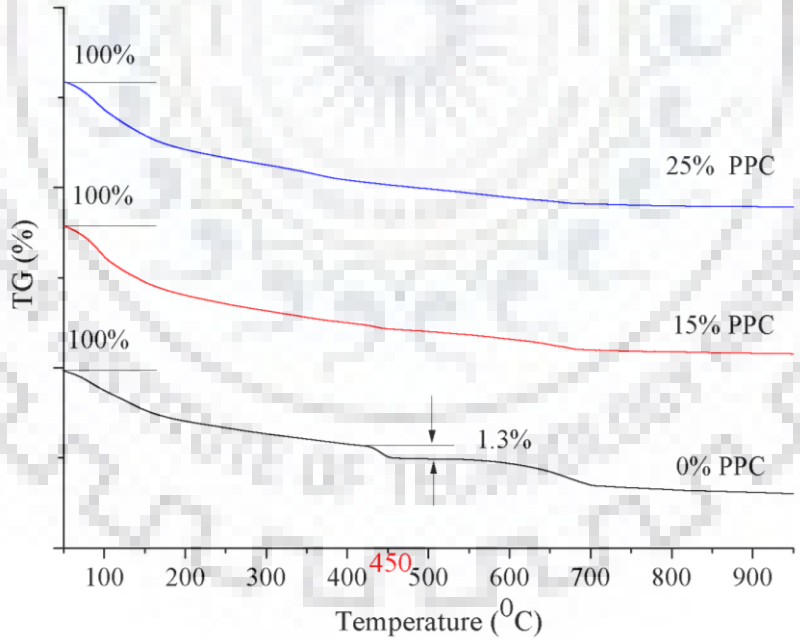

Figure 47: TGA curves of the PPC samples

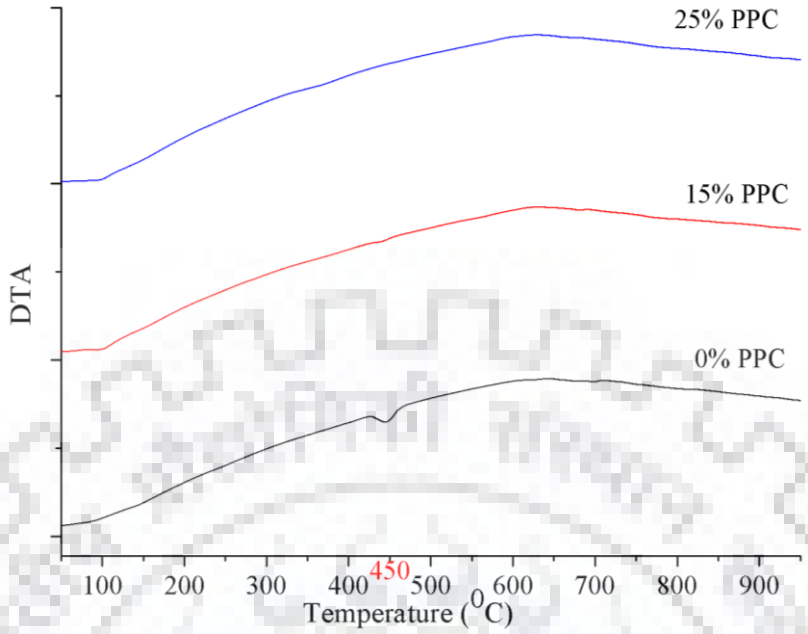

Figure 48: DTA curves for the PPC samples

From the TGA curves of OPC samples in Figure 45, it can be observed that there is a mass loss between 50 ºC and 150 ºC in all the jarosite percentage compositions in OPC i.e. 0%, 15% and 25%. This mass loss is attributed to vaporization of free water in the samples. The mass loss that occurs at 450˚C is due to the decomposition of calcium hydroxide into lime (CaO) and water. It can also be observed that the mass loss at 450˚C becomes less significant with increase in jarosite percentage compositions as it is also evidenced in Figure 46. This implies that there is less amount calcium hydroxide in more jarosite compositions in the OPC. A similar behaviour is also exhibited by PPC samples in Figure 47 and Figure 48.

It can be concluded that the XRD results are in agreement with the TGA-DTA results and it is as well reflected in the results from the pH tests conducted on concrete powdered samples obtained from specimens of both OPC and PPC of the respective jarosite compositions as described in the following section.

4.4 Measurement of the pH

Table 6 shows the pH readings from the pH meter taken after immersing the electrode of the pH meter in a solution of powdered samples obtained from concrete with the respective jarosite compositions.

Table 6: pH values of OPC and PPC concrete with different jarosite percentage compositions.

Percentage composition of jarosite	0%	15%	25%
OPC	12.42	12.31	11.34
PPC	12.17	12.00	11.01

In relation to the table above, the reduction in alkalinity with increase in jarosite composition in both OPC and PPC samples is attributed to the reduction in calcium hydroxide with increase in jarosite composition in both OPC and PPC samples as evidenced from the results of XRD analysis and TGA analysis.

4.5 Permeability

Table 7 and Table 8 show the depth of penetration for water for both OPC and PPC specimens after exposure to water under a pressure of 10kg/cm^2 on the top surface for 100 hours as described for the permeability experiment.

Table 7: Depth of penetration for OPC specimens (cm)

Specimen no.	0% OPC	15% OPC	25% OPC
1	4.5	3.0	1.5
2	4.2	2.5	1.7
Average depth	**4.35**	**2.75**	**1.60**

Table 8: Depth of penetration for PPC specimens (cm)

Specimen no.	0% PPC	15% PPC	25% PPC
1	3.5	1.5	1.0
2	3.2	1.7	1.2
Average depth	**3.35**	**1.60**	**1.10**

The volume of permeable voids for both OPC and PPC specimens has been determined as described in accordance to ASTM C642-97 and the results are presented in Table 9.

Table 9: Volume of permeable voids (%)

Percentage composition of jarosite	0%	15%	25%
OPC	10.89	12.74	16.20
PPC	14.04	15.20	16.42

Table 10: Coefficients of permeability for OPC specimens

Specimen	0% OPC	15% OPC	25% OPC
Porosity	0.1089	0.1274	0.1620
Pressure head (cm)	9.6	6.5	5.6
Kp (m/sec)	**2.98×10^{-9}**	**2.06×10^{-9}**	**1.03×10^{-9}**

T**able 11:** Coefficients of permeability for PPC specimens

Specimen	0% PPC	15% PPC	25% PPC
Porosity	0.1404	0.1520	0.1642
Pressure head (cm)	8.2	5.3	3.4
Kp (m/sec)	**2.67×10^{-9}**	**1.02×10^{-9}**	**8.12×10^{-10}**

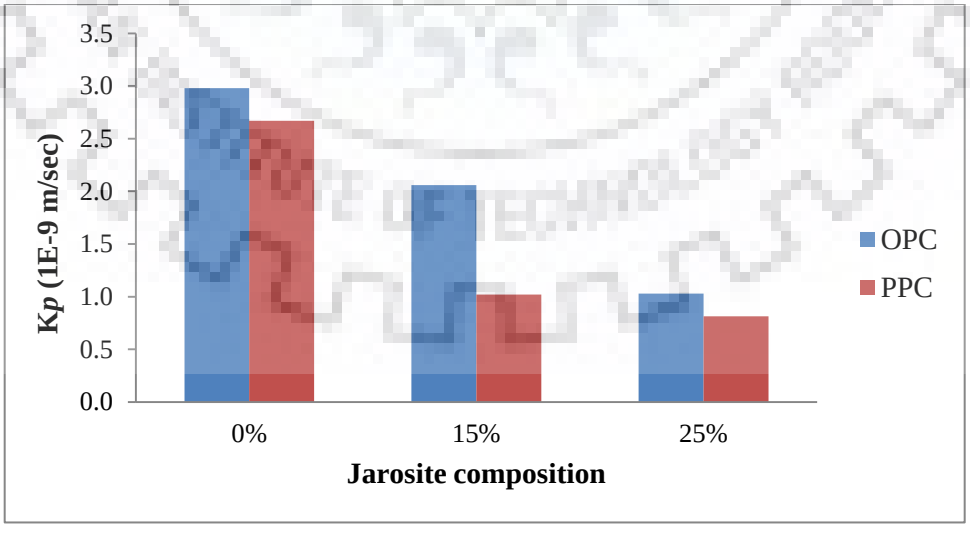

Figure 49: Coefficients of permeability for OPC and PPC specimens

From the results obtained, it has been observed that the values of the coefficient of permeability generally decrease with increase percentage of jarosite replacement of both OPC and PPC with jarosite. This is attributed to jarosite being finer than cement hence acting as a filler material. Consequently, a densely packed microstructure is formed in concrete as more jarosite is added to concrete thus reducing the permeability of the concrete.

4.5 Acid attack

Table 12: Percentage loss in mass of OPC specimens subjected to acid attack

Percentage composition	Mass (g)		Percentage loss
	Before immersion	After immersion	
0%	2469.17	2362.00	4.340
15%	2470.17	2374.00	3.893
25%	2434.00	2364.33	2.862

Table 13: Percentage loss in compressive strength of OPC specimens subjected to acid attack

Percentage composition	Compressive strength (MPa)		Percentage loss
	Control specimen	Immersed specimen	
0%	41.91	27.34	34.76
15%	33.76	23.46	30.51
25%	41.44	30.86	25.53

Table 14: Percentage loss in mass of PPC specimens subjected to acid attack

Percentage composition	Mass (g)		Percentage loss
	Before immersion	After immersion	
0%	2488.83	2414.83	2.973
15%	2452.67	2406.07	1.900
25%	2472.33	2459.00	0.539

Table 15: Percentage loss in compressive strength of PPC specimens subjected to acid attack

Percentage composition	Compressive strength (MPa)		Percentage loss
	Control specimen	Immersed specimen	
0%	33.57	24.41	27.29
15%	35.00	27.11	22.54
25%	32.90	27.20	17.33

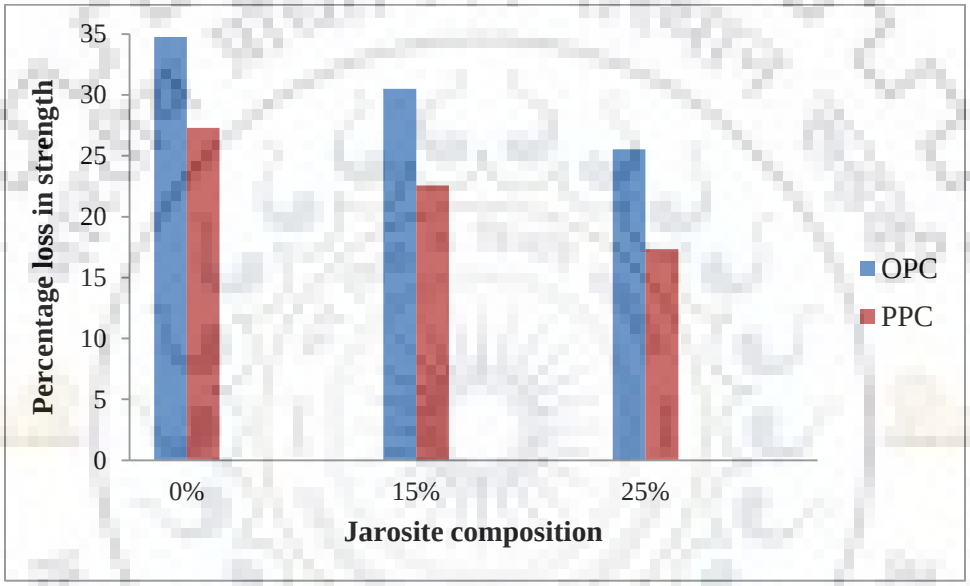

Figure 50: Percentage loss in strength after acid attack for OPC and PPC

From the results obtained, it can be seen that there is a general reduction in mass and strength for both OPC as well as PPC samples. This is attributed to the reaction between sulphuric acid and concrete as follows [7]:

$$Ca(OH)_2 + H_2SO_4 \longrightarrow CaSO_4.2H_2O \text{ ---------- (iv)}$$

$$3CaO.2SiO_2.3H_2O + H_2SO_4 \longrightarrow CaSO_4.2H_2O + Si(OH)_4 \text{ ---------- (v)}$$

However, it can be seen that the percentage loss in mass and strength decreases as the jarosite content increases for both OPC and PPC specimens. This is because jarosite contains silica which reacts with calcium hydroxide produced from the primary hydration reaction to produce more calcium silicate hydrate (CSH). As result, increasing in the jarosite content in the

specimens decreases the amount calcium hydroxide in the specimens available for the reaction according to equation (iv) thus improving the acid resistance properties of the concrete.

4.7 Sulphate attack

Table 16: Percentage loss in compressive strength of OPC specimens after sulphate attack

Percentage composition	Compressive strength (MPa)		Percentage loss
	Control specimen	Immersed specimen	
0%	44.17	36.48	17.410
15%	32.97	29.32	11.071
25%	37.58	34.43	8.382

Table 17: Percentage loss in compressive strength of PPC specimens after sulphate attack

Percentage composition	Compressive strength (MPa)		Percentage loss
	Control specimen	Immersed specimen	
0%	39.80	34.85	12.437
15%	44.96	41.08	8.630
25%	38.97	37.44	3.926

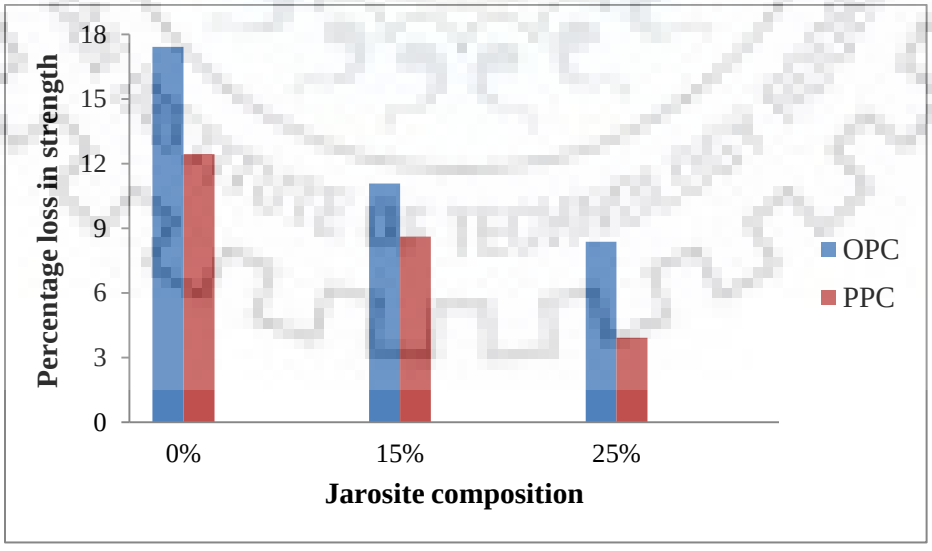

Figure 51: Percentage loss in strength after sulphate attack for OPC and PPC

From Table 16 and Table 17, it can be seen that the percentage loss in strength decreases as the jarosite content increases for both OPC and PPC specimens. This is because both OPC and PPC contain a considerable amount of aluminates compared to jarosite. This implies that as more cement is replaced by jarosite in the specimens, there is a reduction in the quantity of the aluminates available for reaction as per equation (vi) below [6]:

$$2(3CaO.Al_2O_3.12H_2O) + 3(Na_2SO_4.10H_2O) \longrightarrow 3CaO.Al_2O_3.3CaSO_4.32H_2O + 2Al(OH)_3 + 6NaOH + 17H_2O \text{ ---------- (vi)}$$

Addition of jarosite also leads to a secondary reaction between silica and calcium hydroxide in the cement thereby reducing the quantity of calcium hydroxide available for reaction as shown in equation (viii) below [6]:

$$Ca(OH)_2 + Na_2SO_4.10H_2O \longrightarrow CaSO_4.2H_2O + 2NaOH + 8H_2O \text{ ---------- (vii)}$$

The permeability of the concrete is also another significant factor because it governs the rate of penetration of the sulphate solution into the concrete. As the concrete becomes less permeable, the effect of sulphate attack on the concrete becomes less. This has also been confirmed by the results obtained from the permeability tests (Table 10 and Table 11) conducted on the specimens.

4.8 Corrosion

The percentage mass loss of steel reinforcement for both OPC and PPC specimens is provided in Table 18 and Table 19 below. Figure 52 is a graphical representation of percentage loss in mass of steel reinforcement in both OPC and PPC specimens.

Table 18: Mass loss due to corrosion test for OPC specimens

Specimen no.	**0% OPC**		**15% OPC**		**25% OPC**	
	Mass loss	**Average mass loss**	**Mass loss**	**Average mass loss**	**Mass loss**	**Average mass loss**
1	6.04%	**13.74%**	10.67%	**14.23%**	18.33%	**21.67%**
2	11.54%		14.61%		32.78%	
3	23.63%		17.42%		13.89%	

Table 19: Mass loss due to corrosion test for PPC specimens

Specimen no.	0% PPC		15% PPC		25% PPC	
	Mass loss	Average mass loss	Mass loss	Average mass loss	Mass loss	Average mass loss
1	8.15%	**6.09%**	7.58%	**6.09%**	8.99%	**9.93%**
2	3.09%		7.30%		11.52%	
3	7.02%		3.37%		9.27%	

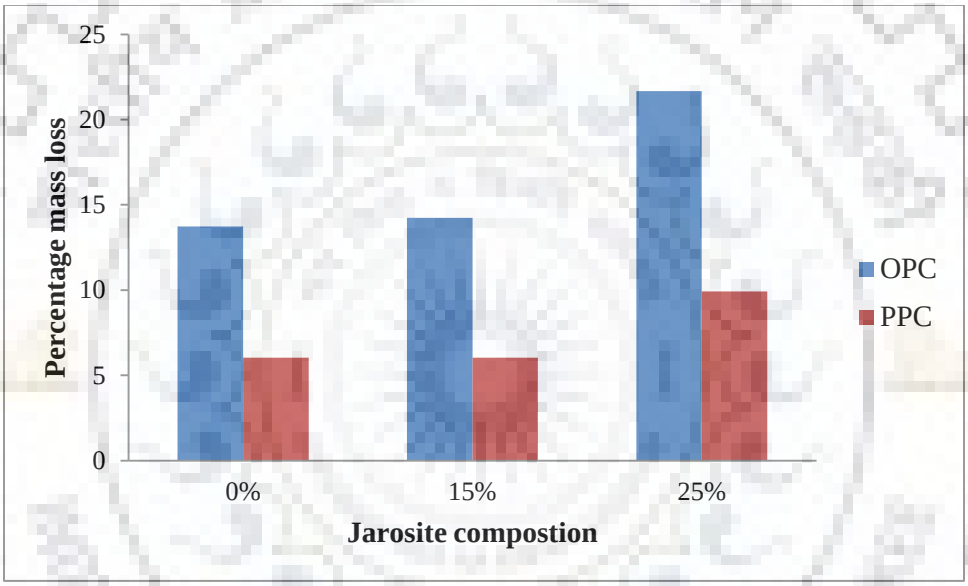

Figure 52: Percentage mass loss due to corrosion in OPC and PPC

From the results in Table 18, it can be observed that the replacement of OPC with jarosite by 15% does not have any significant effect on the mass loss while the increase in replacement of OPC with jarosite from 15% to 25% showed increase in the mass loss due to corrosion. A similar behaviour is also shown with PPC in Table 17 i.e. there is no significant effect on the mass loss when PPC is replaced with jarosite by 15% but the increase in replacement of PPC with jarosite from 15% to 25% showed an increase in the mass loss due to corrosion. This is because the compositions of 0% and 15% jarosite have pH values above 12 (Table 6) which is the minimum pH value sufficient for the passivation of steel reinforcement in concrete against corrosion while the composition of 25% jarosite shows pH values of 11.34 and 11.01 for OPC and PPC respectively hence the increase in the rate of corrosion.

In addition, there is more mass loss due to corrosion in OPC as compared to PPC. This is so because for corrosion of reinforcement to occur, a critical quantity of chloride is required at the steel-concrete interface. In OPC, the critical quantity of chloride required is reached in a short time as compared to PPC. This is attributed to the formation of a more packed structure in PPC due to production of more CSH gel from the pozzolanic reaction which does not happen in OPC. As a result, the permeability of PPC concrete is less than that of OPC concrete hence water containing chloride ions takes a longer time to reach the steel-concrete interface in PPC concrete.

4.9 Marine application

Table 20: Chloride content at different depths of PPC specimen

Depth from the surface (mm)	0% PPC	15% PPC	25% PPC
0	0.4413	0.4815	0.4466
5	0.3200	0.4597	0.3482
10	0.2241	0.3203	0.3043
15	0.1000	0.2190	0.2254
20	0.0704	0.1353	0.1295
25	0.0631	0.0632	0.0609

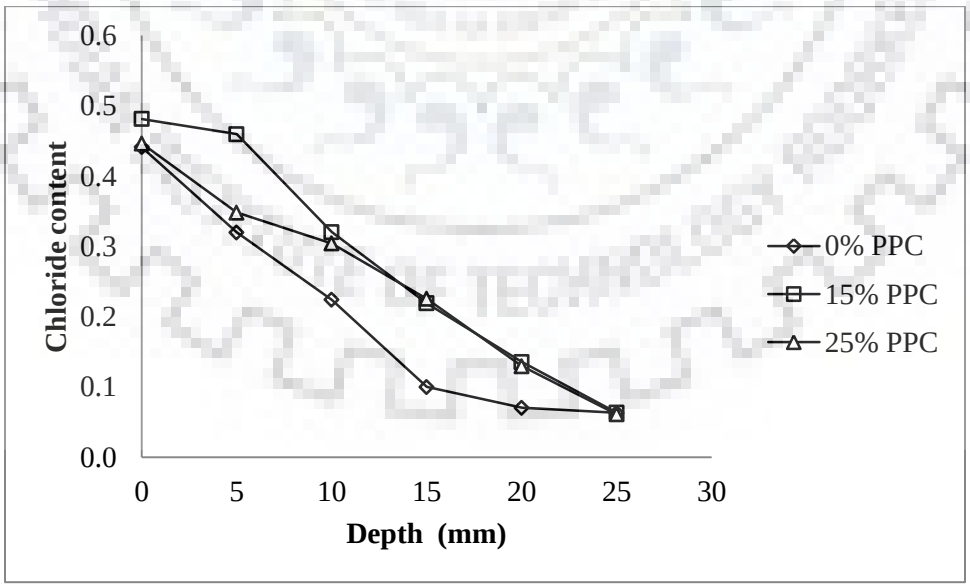

Figure 53: A graph of chloride content versus depth

From Figure 53, it can be seen that there is no significant effect on the chloride penetration at all jarosite compositions in PPC. The slight deviations are in the chloride content are because of the pores in concrete. The pores are filled up with NaCl solution during ingression and hence there are variations in the chloride content at different depths.

4.10 Elevated temperature studies

Elevated temperature is well known for damaging concrete micro- and meso-structure which leads to mechanical deterioration of the concrete and even detrimental effects at the structural level due to concrete spalling and bar exposure to the flames in case of fire [8]. The fire response of concrete structural members is dependent on the thermal, mechanical and deformation properties of concrete. These properties vary significantly with temperature and also depend on the composition and characteristics of concrete batch mix as well as heating rate and other environmental conditions [9].

The physical and chemical changes that occur in the concrete microstructure when exposed to high temperature can be described as follows; hydration products lose free water and chemically bonded water at 105ºC while capillary water is completely lost at 400ºC. Above 350ºC, calcium hydroxide decomposes into lime and water while CSH starts to decompose at 560ºC [8].

As a result of evaporation of water and chemical changes of the hydration products, elevation of temperature increases the porosity and pore size of the concrete. The coarsening of the pore structure contributes to the deterioration of mechanical properties in concrete at elevated temperature [8].

For case of the microstructure, no micro-cracks are formed up to 200ºC in either the cement matrix or the interfacial transitional zone. However when the temperature rises to 400ºC, micro-cracks start to propagate in the cement matrix and the interfacial transitional zone and their intensity increases with rise in temperature. As the temperature increases, the hardened cement matrix shrinks as a result of loss of water while the aggregates expand [8].

Consequently strains are developed which produce stresses between the cement matrix and the aggregates causing micro-cracks in the interfacial transitional zone. This is also another factor responsible for the deterioration of mechanical properties of concrete at elevated temperature [8].

4.11 Compressive strength

The compressive strength results for OPC and PPC specimens are presented in Table 21 and Table 22 respectively while the percentage loss in strength due to exposure to elevated temperature is presented in Table 23 together with Figure 54 and Figure 55. All samples exposed to elevated temperature have been tested after cooling down to ambient temperature and therefore the compressive strength results obtained correspond to the residual compressive strength and not the high temperature compressive strength.

Table 21: Compressive strength of OPC specimens (MPa)

Percentage composition	**Temperature of exposure**		
	Ambient	**350ºC**	**600ºC**
0%	28.62	24.45	12.22
15%	25.92	14.66	7.68
25%	28.78	13.44	7.02

Table 22: Compressive strength of PPC specimens (MPa)

Percentage composition	**Temperature of exposure**		
	Ambient	**350ºC**	**600ºC**
0%	32.21	27.51	13.52
15%	30.13	17.44	8.78
25%	31.77	15.05	7.72

Table 23: Percentage loss in compressive strength for OPC and PPC specimens

Percentage composition	**350ºC**		**600ºC**	
	OPC	**PPC**	**OPC**	**PPC**
0%	14.57	14.59	57.30	58.03
15%	43.44	42.12	70.37	70.86
25%	53.30	52.63	75.61	75.70

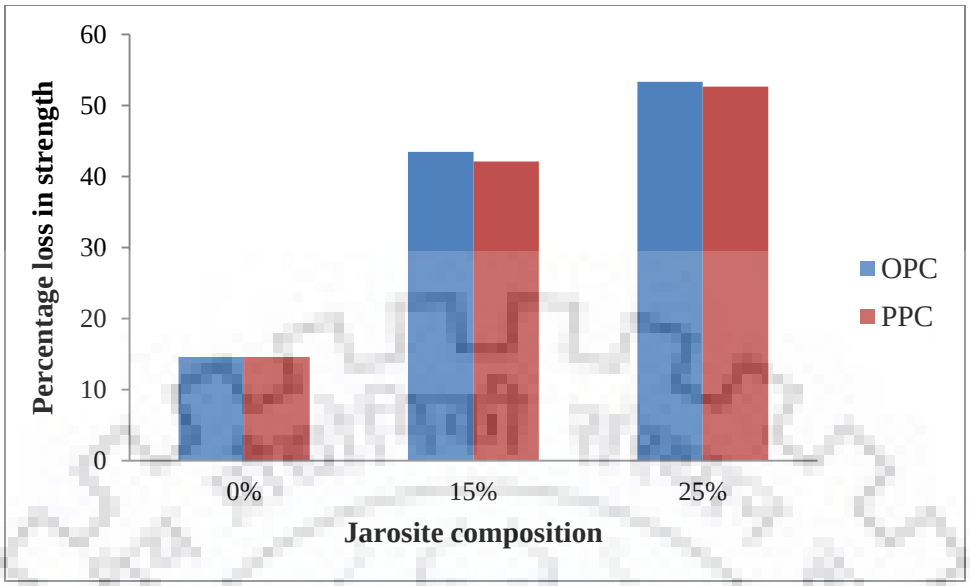

Figure 54: Percentage loss in strength for OPC and PPC at 350ºC

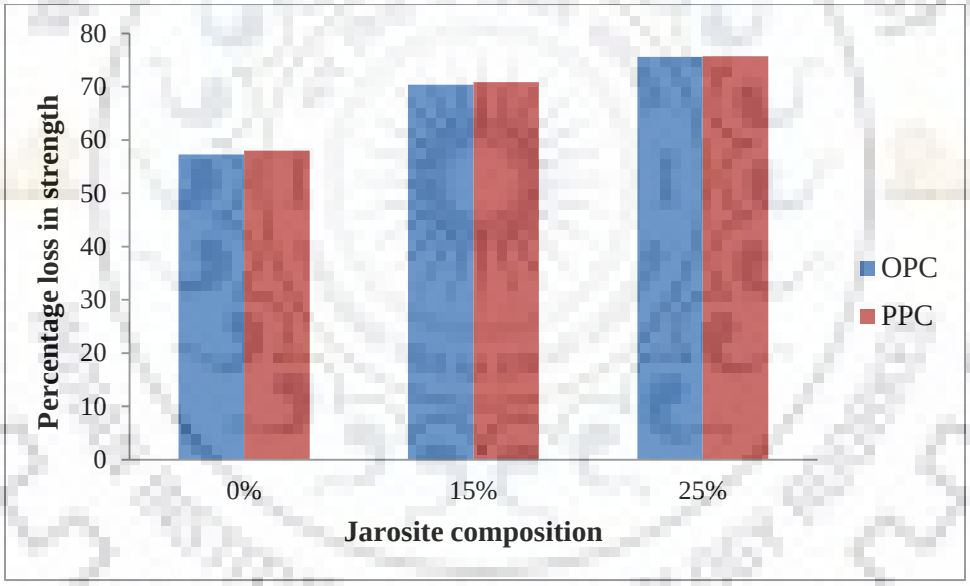

Figure 55: Percentage loss in strength for OPC and PPC at 600ºC

From the results obtained, it can be observed that the percentage loss in strength due to exposure to high temperature increases with the increase in the jarosite content i.e. there is a higher percentage loss in strength in concrete specimens containing jarosite as compared to the concrete specimens without jarosite. This is so because addition of jarosite to concrete leads to formation of a compact dense microstructure.

Under high temperature, the compact microstructure does not allow moisture to escape easily hence resulting in the build-up of pore pressure and rapid development of micro-cracks leading to a faster decrease in strength and spalling [9].

Another experiment has been carried out in which three replacement levels of 0%, 15% and 25% have been considered for OPC and PPC with three specimens of each replacement level heated up to 350ºC and 600ºC at a rate of at a rate of 5ºC per minute. After reaching the target temperature, the specimen is left in the furnace for three hours to attain steady state. Thereafter the furnace is switched off and the sample is left inside to cool down gradually and then tested for compressive strength under displacement control. The residual compression test results obtained are shown in Table 24 and Table 25. Explosive spalling was encountered in PPC specimens with jarosite compositions of 15% and 25% as shown in Table 25 due to exposure to high rate of temperature rise. Figure 56 shows one of the specimens after explosive spalling.

Table 24: Compressive strength of OPC specimens (MPa)

Percentage composition	**Temperature of exposure**		
	Ambient	**350ºC**	**600ºC**
0%	31.16	26.84	19.42
15%	28.22	16.30	11.38
25%	20.92	7.41	5.38

Table 25: Compressive strength of PPC specimens (MPa)

Percentage composition	**Temperature of exposure**		
	Ambient	**350ºC**	**600ºC**
0%	33.39	28.96	22.07
15%	32.34	20.74	Explosive spalling
25%	20.50	Explosive spalling	Explosive spalling

Figure 56: One of the specimens after explosive spalling

The explosive spalling encountered Table 25 is attributed to the rapid build-up of pore pressure and thermal stresses due to the high rate of temperature rise which results into propagation of micro-cracks at a faster rate with high intensity in the concrete.

4.12 Modulus of Elasticity

The modulus of elasticity for concrete specimens after exposure to high temperature has been tested as described in section 3.12 and the results are presented in Table 26 and Table 27 for both OPC and PPC specimens respectively while the percentage loss in modulus of elasticity is shown in Table 28 together with Figure 57.

Table 26: Modulus of elasticity of OPC specimens (N/mm^2)

Percentage composition	Temperature of exposure		
	Ambient	**350°C**	**600°C**
0%	33466.36	18805.68	1043.87
15%	33319.56	11901.31	1013.23
25%	33386.23	11499.25	1006.74

Table 27: Modulus of elasticity of PPC specimens (N/mm^2)

Percentage composition	Temperature of exposure		
	Ambient	350ºC	600ºC
0%	36467.64	20527.02	1047.72
15%	35131.36	12727.12	1011.96
25%	35271.74	12397.37	1005.87

Table 28: Percentage loss of modulus of elasticity for OPC and PPC specimens

Percentage composition	350ºC		600ºC	
	OPC	PPC	OPC	PPC
0%	43.81	43.71	96.88	97.13
15%	64.28	63.77	96.96	97.12
25%	65.56	64.85	96.98	97.15

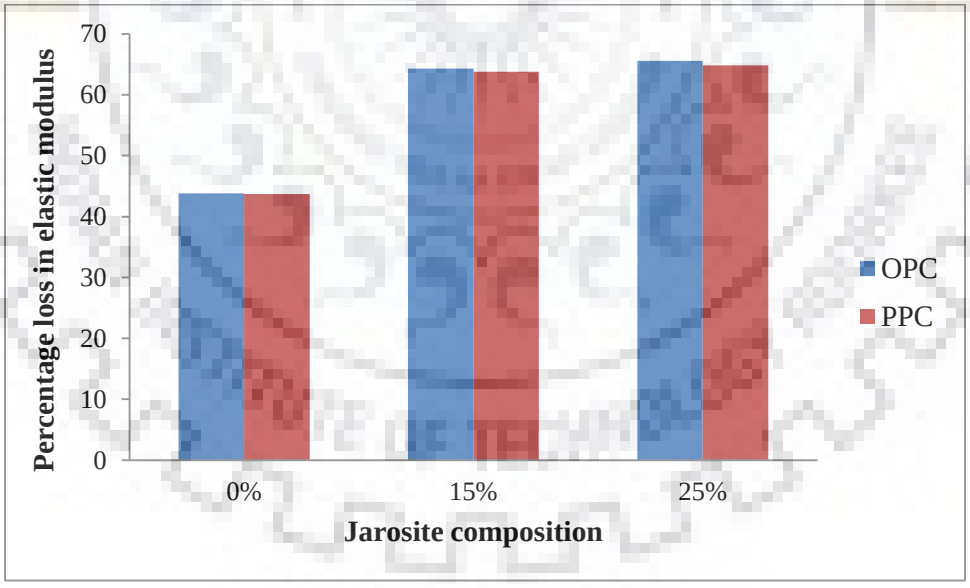

Figure 57: Percentage loss in modulus of elasticity for OPC and PPC at 350ºC

From the results obtained, it can be seen that there is a more percentage loss at 350ºC in the modulus of elasticity of concrete containing jarosite compared to the control specimens. This is so because addition of jarosite to concrete leads to formation of a compact dense microstructure.

Under high temperature, the compact microstructure does not allow moisture to easily escape resulting in the build-up of pore pressure and thereby creating excessive thermal stresses.

In addition, it can be seen that at 600ºC all the specimens have lost more than 90% of their modulus of elasticity. This significant reduction in the modulus of elasticity is attributed to the excessive thermal stresses as well as the physical and chemical changes that occur in the concrete microstructure as discussed in section 4.10

4.13 Stress-strain relationship

Generally, due to the decrease in compressive strength of concrete, the slope of stress-strain curve decreases with increase in temperature. The strength of concrete has a significant influence on stress-strain response both at room and elevated temperatures [9]. As the temperature increases in normal concrete, stress-strain curves become flatter and the peak stress shifts downwards and rightwards as seen in Figure 58. These indicate that the peak stress and the modulus of elasticity of concrete decrease with the increase in temperature but the strain at peak stress increases with temperature [8]. The variation of the stress-strain relationship with increase temperature in concrete containing jarosite is shown in Figure 59, Figure 60, Figure 61 and Figure 62.

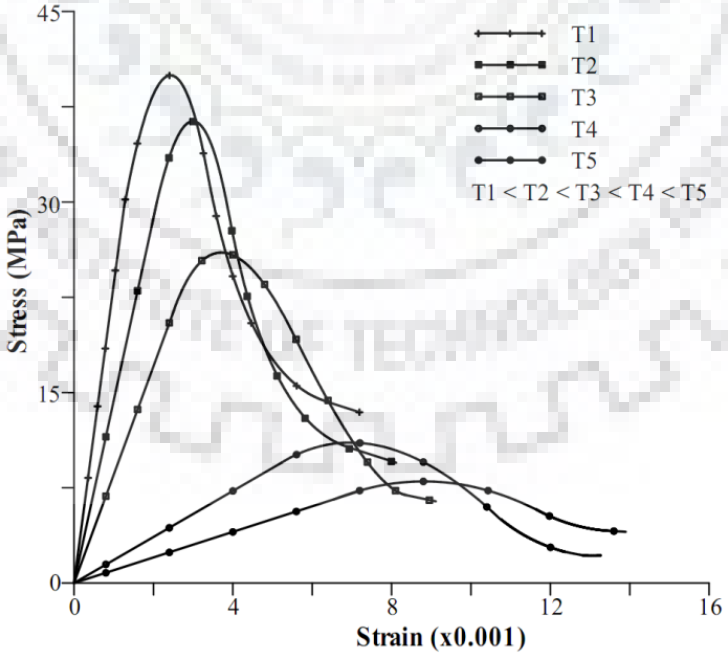

Figure 58: Stress-strain relationship of concrete at elevated temperatures

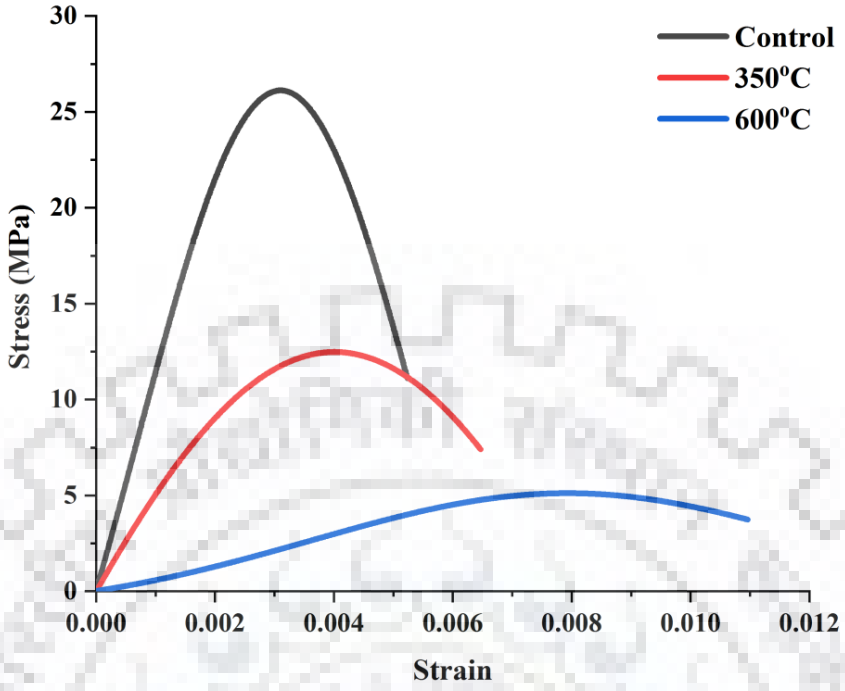

Figure 59: Stress-strain relationship for 15% OPC

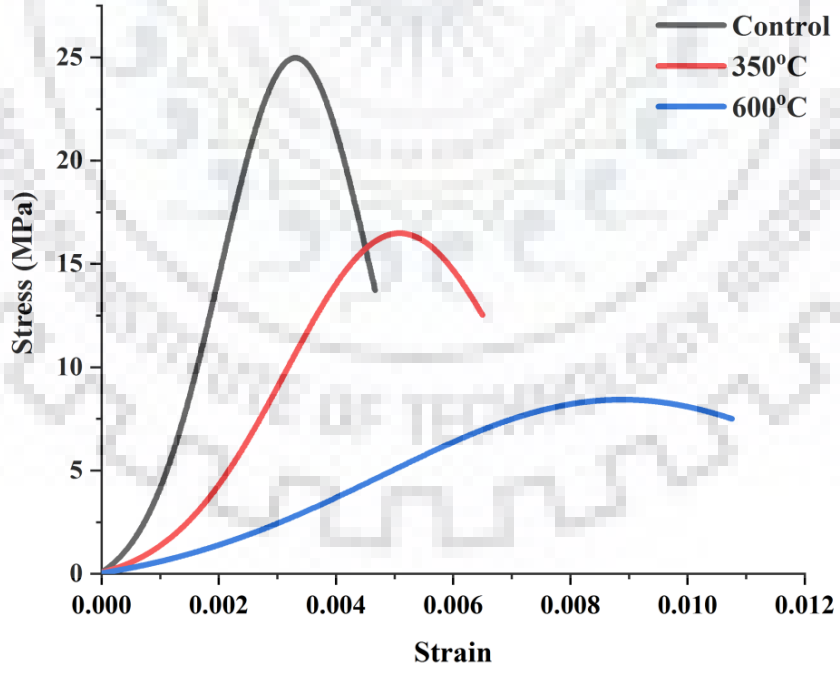

Figure 60: Stress-strain relationship for 15% PPC

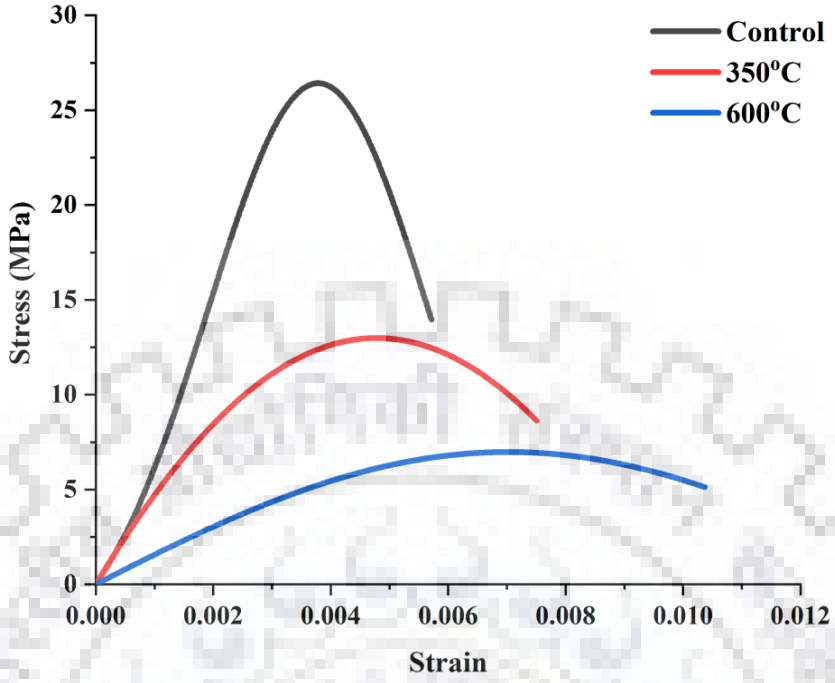

Figure 61: Stress-strain relationship for 25% OPC

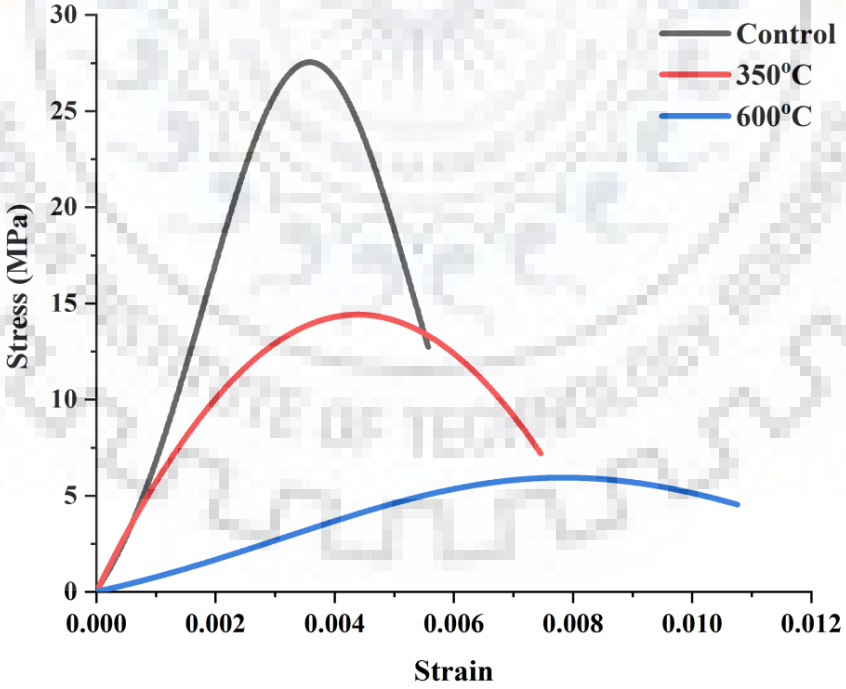

Figure 62: Stress-strain relationship for 25% PPC

From the results obtained, it can be seen that variation of the stress-strain relationship with increase in temperature in concrete containing jarosite is similar to that of normal concrete i.e. the peak stress and the modulus of elasticity of concrete decrease with increase in temperature but the strain at peak stress increases with temperature which is also seen in normal concrete. In addition, it also is observed that there is an increase in the strain as the temperature increases which is seen in normal concrete. This is attributed to development of micro-cracks in concrete as the temperature increases which is also experienced in normal concrete. It can therefore be concluded that jarosite does not affect the stress-strain relationship of concrete on exposure to high temperature.

CHAPTER FIVE

CONCLUSION

5.1 Summary

Jarosite has a retarding effect on the hydration process of cement (OPC and PPC). This is as a result of the formation of ettringite due to the substantial amount of SO_3 contained in jarosite and also jarosite grains being finer than cement grains thus creating a diffusion barrier around cement grains and hence slowing down the hydration. However it has been seen that the overall effect is exaggerated in PPC.

Experiments have also shown that jarosite gives better hydration after the acceleration peak in the later stages of hydration. This is due to the reaction between the silica (SiO_2) in jarosite and the calcium hydroxide ($Ca(OH)_2$) produced from the primary hydration to produce more calcium silicate hydrate (CSH).

In relation to the above, as more jarosite is added to cement, the quantity of calcium hydroxide in the cement decreases which also leads to reduction in the alkalinity of the concrete. This has been confirmed by XRD analysis and TGA analysis as well as pH tests conducted on the concrete containing jarosite.

Permeability tests have proved that jarosite improves the permeability properties of concrete. This is as a result of having finer grains than cement hence acting as a filler material in the concrete. Consequently, a more densely packed microstructure is achieved with addition of jarosite to the concrete.

Jarosite has also been found to improve the acid resistance of concrete. This is due to the consumption of calcium hydroxide ($Ca(OH)_2$) in the secondary reaction due to the presence of silica (SiO_2) in jarosite hence reducing the amount of calcium hydroxide ($Ca(OH)_2$) in the concrete available for reaction with acids.

It has also been seen that jarosite improves the sulphate resistance properties in concrete. This is so because addition of jarosite reduces the amount of aluminates in the concrete as well as calcium hydroxide available for reaction. The reduction in the permeability with addition of jarosite is also another factor which plays an important role by reducing the rate of penetration of water containing sulphates thus minimizing the effect of sulphate attack in the concrete.

Corrosion tests have shown that addition of jarosite to concrete increases the rate of corrosion of reinforcement. However, it has also been observed that there is no significant difference in mass loss between 15% composition and the controls whereas at 25% the mass loss is significant. This is attributed to the reduction in the alkalinity of the concrete as the percentage composition of jarosite increases as indicated by the results obtained from the pH tests.

According to the results obtained from elevated temperature studies, it has been found that addition of jarosite increases the percentage loss in strength of concrete when exposed to high temperature. This is because a compact dense structure is formed in concrete containing jarosite which does not allow moisture to escape easily due to the low permeability hence resulting in the build-up of pore pressure and rapid development of micro-cracks leading to a faster decrease in strength and spalling.

In relation to the above, excessive thermal stresses are created leading to a more percentage loss in the modulus of elasticity at 350ºC compared to the control specimens. However at 600ºC, there is a significant reduction in the modulus of elasticity of all the specimens including the control specimens.

Elevated temperature studies have also shown that variation of the stress-strain relationship with increase in temperature in concrete containing jarosite is similar to that of normal concrete. Therefore it can be concluded that jarosite does not affect the stress-strain behaviour of concrete on exposure to high temperature.

REFERENCES

1. Asokan Pappua, Mohini Saxena, Shyam R. Asolekar (2006) 'Jarosite characteristics and its utilisation potentials', *Science of the Total Environment*, 359(1–3), pp. 232–243.
2. M. Patrick Mubiayi, M. Elizabeth Makhatha, and E. Titilayo Akinlabi, "Characterization, leachate Characteristics and compressive strength of Jarosite/clay/fly ash bricks," *Mater. Today Proc.*, vol. 5, no. 9, pp. 17802–17811, 2018.
3. A.K.Vyas (2011) 'Solidification- Stabilization Technique for Metal bearing Solid Waste from Zinc Industry – A case study', 19, pp. 151–155.
4. Priyansha Mehra, Ramesh Chandra Gupta, Blessen Skariah Thomas (2016) 'Properties of concrete containing jarosite as a partial substitute for fine aggregate', *Journal of Cleaner Production*, 120, 241-248.
5. V. Saraswathy, S. Karthick, H. S. Lee, S.-J. Kwon, and H.-M. Yang, "Comparative Study of Strength and Corrosion Resistant Properties of Plain and Blended Cement Concrete Types," *Adv. Mater. Sci. Eng.*, vol. 2017, pp. 1–14, 2017
6. Neville, A. M. (2013). *Properties of concrete*. Fifth Edition. New Delhi: Dorling Kindersely India Pvt. Ltd.
7. Hadigheh, S. A., Gravina, R. J. and Smith, S. T. (2017) 'Effect of acid attack on FRP-to-concrete bonded interfaces', *Construction and Building Materials*. Elsevier Ltd, 152, pp. 285–303.
8. Q. Ma, R. Guo, Z. Zhao, Z. Lin, and K. He, "Mechanical properties of concrete at high temperature-A review," Constr. Build. Mater., vol. 93, pp. 371–383, 2015.
9. V. Kodur, "Properties of Concrete at Elevated Temperatures," ISRN Civ. Eng., vol. 2014, pp. 1–15, 2014.
10. R. P. Khatri and V. Sirivivatnanon (1997) 'Methods for the determination of water permeability of Concrete', *ACI Materials Journal*, 94(3), pp. 257-261.
11. IS: 10262-2009 (2009) 'Concrete Mix Proportioning - Guidelines', *Bureau of Indian Standards, New Delhi*.
12. IS 3085- 1965 (1965) 'Permeability of Cement Mortar', *Bureau of Indian Standard, New Delhi*.
13. ASTM C469-14 (2014) 'Standard Test Method for Static Modulus of Elasticity and Poisson's Ratio of Concrete in Compression', *ASTM International*, pp. 1–5.